



1 **Ocean acidification enhances primary productivity and**
2 **nocturnal carbonate dissolution in intertidal rock pools**

3

4 **Narimane Dorey^{1, †}, Sophie Martin^{2, 3}, Lester Kwiatkowski⁴**

5

6 ¹ LMD-IPSL, CNRS, Ecole Normale Supérieure/PSL Res. Univ, Ecole Polytechnique, Sorbonne
7 Université, Paris, 75005, France

8 ² CNRS, UMR7144, Station Biologique, Place Georges Teissier, 29688 Roscoff Cedex, France

9 ³ Laboratoire Adaptation et Diversité en Milieu Marin, Sorbonne Universités, UPMC Univ Paris
10 06, Station Biologique, Place Georges Teissier, 29688 Roscoff Cedex, France

11 ⁴ LOCEAN Laboratory, Sorbonne Université-CNRS-IRD-MNHN, Paris, 75005, France

12

13 [†] Correspondence to: Narimane Dorey

14 Ecole Normale Supérieure,

15 Département de Géosciences,

16 24 rue Lhomond, 75005 Paris, France

17 E-mail: narimane.dorey@gmail.com

18



19 ABSTRACT

20 Human CO₂ emissions are modifying ocean carbonate chemistry, causing ocean acidification, and
21 likely already impacting marine ecosystems. In particular, there is concern that coastal, benthic
22 calcifying organisms will be negatively affected by ocean acidification, a hypothesis largely
23 supported by laboratory studies. The inter-relationships between carbonate chemistry and marine
24 calcifying communities *in situ* are complex and natural mesocosms such as tidal pools can provide
25 useful community-level insights. In this study, we manipulated the carbonate chemistry of
26 intertidal pools to investigate the influence of future ocean acidification on net community
27 production (NCP) and calcification (NCC) at emersion. Adding CO₂ at the start of the tidal
28 emersion to simulate future acidification (+1500 μatm pCO₂, target pH: 7.5) modified net
29 production and calcification rates in the pools. By day, pools were fertilized by the increased CO₂
30 (+20 % increase in NCP, from 10 to 12 mmol O₂ m⁻² hr⁻¹), while there was no measurable impact
31 on NCC. During the night, pools experienced net community dissolution (NCC < 0), even in
32 present-day conditions, when waters were supersaturated with regards to aragonite. Adding CO₂
33 in the pools increased nocturnal dissolution rates by 40% (from -0.7 to -1.0 mmol CaCO₃ m⁻² hr⁻¹)
34 with no consistent impact on night community respiration. Our results suggest that ocean
35 acidification is likely to alter temperate intertidal community metabolism on sub-daily timescales,
36 enhancing both diurnal community production and nocturnal calcium carbonate dissolution.

37 SHORT SUMMARY

38 Human CO₂ emissions are modifying ocean carbonate chemistry, causing ocean acidification, and
39 likely already impacting marine ecosystems. Here, we added CO₂ in intertidal pools at the start of
40 emersion to investigate the influence of future ocean acidification on net community production
41 (NCP) and calcification (NCC). By day, adding CO₂ fertilized the pools (+20 % NCP). By night,
42 pools experienced net community dissolution, a dissolution that was further increased (+40 %) by
43 the CO₂ addition.

44 **Keywords:** Ocean acidification, calcification, coralline algae, mesocosms, primary production,
45 temperate community, tidal pool



46 INTRODUCTION

47 The ongoing increase of anthropogenic carbon dioxide (CO₂) in the atmosphere and the ocean –
48 resulting in ocean acidification - is likely to create adverse living conditions for marine coastal
49 communities (IPCC, 2019). Ocean acidification is projected to further decrease average surface
50 pH by up to 0.4 units by 2100 (Kwiatkowski et al., 2020), and is identified as a major threat to
51 marine ecosystems (IPCC, 2019). Lower seawater pH has significant effects on marine organisms
52 physiology and fitness: from altered survival and reduced growth (see review by Kroeker et al.
53 2013), to changes in pH homeostasis (e.g., Kottmeier et al., 2022), metabolic rates, and energy
54 trade-offs (e.g., Dorey et al., 2013; Pan et al., 2015) and reduced feeding efficiency (e.g., Stump
55 et al., 2013). Marine calcifiers - the builders of calcified structures (CaCO₃) - have been a focus of
56 ocean acidification research due to the sensitivity of calcification to the carbonate saturation state
57 (Ω), defined as follows:

$$58 \quad \Omega = [\text{Ca}^{2+}] [\text{CO}_3^{2-}] / K'_{\text{sp}}$$

59 where K'_{sp} is the stoichiometric solubility product for the considered carbonate polymorph (i.e.,
60 Ω_{a} for aragonite or Ω_{c} for calcite). The saturation state depends on temperature, pH, and pressure
61 (lower Ω when pH or temperature decreases and pressure increases). When $\Omega < 1$, inert carbonate
62 minerals tend to dissolve. The polymorphs composing the calcified structure like calcite and to a
63 greater extent aragonite and high-magnesium calcite, are prone to dissolution when pH decreases.
64 For instance, in Atlantic surface waters (at 20°C), saturation state equilibrium ($\Omega = 1$) is reached
65 at pH 7.3 ($p\text{CO}_2 = 2650 \mu\text{atm}$) for calcite but at pH 7.6 (1250 μatm) for aragonite. For high-
66 magnesium calcite, experiments from (Yamamoto et al., 2012) demonstrate that inert (dead) high-
67 magnesium calcite from coralline algae passively dissolves at Ω_{a} values between 3.0 and 3.2 (also
68 see Ries et al. 2016). Organisms with calcified structures are thus likely to experience reduced net
69 calcification due to ocean acidification, both through enhanced dissolution, and reduced gross
70 calcification rates.

71 Aside from acidifying the ocean (increased H⁺), increased ocean CO₂ uptake could affect
72 the productivity of algae and marine plants. As CO₂ dissolves in the ocean, the dissolved inorganic
73 carbon (DIC: CO₂, HCO₃⁻ and CO₃²⁻) concentration increases. DIC is the substrate for marine
74 photosynthesis (mainly CO₂ and HCO₃⁻), and as such, it can limit photosynthetic rates when scarce.



75 In algae and marine plants that are carbon limited (permanently or periodically), elevated DIC
76 could also directly increase photosynthetic rates and Mackey et al., (2015) propose that these rates
77 could be further increased by the higher concentration gradient between water and the
78 photosynthetic cells. However, the authors point out that while positive effects are theoretically
79 expected, they may be small, specific to species' biology and the environment they live in, and
80 difficult to predict (see also Hurd et al., 2019). In terrestrial ecosystems, the Intergovernmental
81 Panel on Climate Change defines CO₂ fertilization as 'the enhancement of plant growth as a result
82 of increased atmospheric CO₂ concentration' (Jia et al., 2019) and reports that CO₂ fertilization
83 has likely already happened, although the magnitude of this effect depends on the plants, or
84 assemblages/ecosystems considered (and on other factors constraining growth).

85 The response of single species to changes such as ocean acidification and increased DIC
86 concentrations are often insufficient to predict community-level impacts. Ecological interactions
87 such as competition or predation can affect the outcome of perturbation experiments (Kroeker et
88 al., 2012). For instance, Paiva et al. (2021) showed that the laboratory growth of an isopod species
89 was an order of magnitude slower than when raised in the presence of other species from its
90 community. In another study, Legrand et al. (2019) showed that the presence of grazers increased
91 coralline algal calcification (+50% in winter and +100% in summer), but when grazers were
92 combined with ocean acidification, algal calcification decreased more than with acidification
93 alone. Not taking into account such interactions can therefore result in poorly characterizing the
94 effects of ocean acidification. Furthermore, while critical for a mechanistic understanding of the
95 processes affecting marine biota, laboratory studies are seldom realistic. Typically performed in
96 controlled, simplified, and stable conditions (e.g., with respect to temperature and food), laboratory
97 studies can better assess the effect of pH alone (Widdicombe et al., 2010). However exposure to a
98 stable pH (e.g., 7.6 vs. 8.0), fails to reflect the daily and seasonal variability observed in natural
99 ecosystems, in particular coastal ones (Torres et al., 2021). Natural mesocosm perturbation
100 experiments are thus essential tools to investigate future changes in variable and complex
101 ecosystems, difficult to capture in the lab (Andersson et al., 2015; Barry et al., 2010).

102 Most *in situ* mesocosm experiments investigating the effect of ocean acidification have
103 been conducted on planktonic communities, kept in large "bags" equilibrated to the desired pH
104 (Riebesell et al., 2013). These studies demonstrate that adding CO₂ can significantly change the



105 organization of the plankton community (Spisla et al., 2021), and increase autotrophic biomass in
106 high-nutrient conditions (Schulz et al., 2013). Due to the technical challenges, however, benthic
107 calcifying communities are seldom manipulated this way *in situ* (Widdicombe et al., 2010). Two
108 such manipulation experiments are the studies by Albright et al. (2016, 2018), where the authors
109 used NaOH and CO₂ to reproduce pre-industrial and future pH conditions on a coral reef and found
110 evidence that reef growth had been reduced by 7% over the industrial era and was likely to decline
111 further. Other studies have investigated such community-level effects by either simulating
112 “artificial”, simpler, assemblages in laboratory setups (e.g., Cox et al., 2015; Pansch et al., 2016)
113 or using phenomena such as natural CO₂ vents. For instance, in the vents of Ischia, as pH decreases,
114 the presence of calcifying species declines (see review by Foo et al., 2018). Alternatively,
115 Kwiatkowski et al. (2016) used locally-induced acidification due to respiration (no CO₂ addition)
116 in tidal pools, a naturally closed system, and demonstrated that nighttime dissolution of these
117 communities was positively correlated with Ω . Here, we used tidal pools of the English Chanel as
118 ephemeral mesocosms, where we modified carbonate chemistry conditions at the start of emersion
119 through CO₂ addition.

120 Temperate rocky tidal pools - or rockpools - are highly dynamic systems that have been long
121 studied by naturalists since they are easy to reach and their ecosystem structure generally resemble
122 subtidal benthic communities (Ganning, 1971). Tidal pool organisms from the upper shore, well-
123 adapted to pool conditions, form typical benthic communities: often low in diversity, they consist
124 of a few characteristic macroalgal (e.g., *Ulva sp.*) and animal species (e.g., limpets). In winter, red
125 macroalgae – including calcifying algae – often dominate the pools and while they do not disappear
126 in summer, a bloom of soft green macroalgae is generally observed during the warm season.
127 Temperature, salinity, oxygen, and pH in the pools are extremely variable, often far outside the
128 seasonal range of nearby free-flowing seawater (Legrand et al., 2018; Morris & Taylor, 1983).
129 Tidal pools generally emerge from the ocean twice a day in regions of semidiurnal tides with the
130 duration dependent on shore location and the tidal coefficient. On short timescales tidal pools act
131 as closed systems, with carbonate chemistry easily manipulated and temporal changes reflecting
132 *in situ* community metabolism (no water mass transport and negligible air-sea gas exchange).

133 In the present study, we used tidal pools as natural mesocosms to investigate the effect of ocean
134 acidification on communities dominated by calcifying red algae. We measured diurnal and



135 nocturnal net community calcification and production (or respiration) following CO₂ addition
136 across three seasons (winter, spring, and summer), to assess how tidal pool community metabolism
137 may respond to end of the 21st century high ocean acidification (pH 7.5).

138

139 MATERIAL AND METHODS

140 Field site

141 The experiments were performed on a rocky intertidal shore characterized by granitic substrate on
142 the North coast of Brittany, France, between 2019 and 2021. The beach of Bloscon (48°43'30.0"N
143 3°58'10.5"W) is situated in Roscoff at the entrance of the Bay of Morlaix and has a hydrology
144 principally affected by the waters of the English Channel and to a lesser extent the Penzé and
145 Morlaix rivers (**Fig. 1**). This area is characterized by strong, oscillating, semidiurnal tides of up to
146 9 m. Temperatures are generally low in the deeper flowing water (from 9-10 °C in winter to 16-17
147 °C in summer), and salinity is close to that of the adjacent Atlantic (~35; see **Supp. Mat. Fig. S1**
148 for detailed temperature and salinity data from the two nearby SOMLIT monitoring stations
149 Estacade and Astan, a network described in Cocquempot et al., 2019).

150 Tidal pool characterization

151 For this study, we chose five tidal pools with high coverage in calcifying algae ($\geq 30\%$ of the pool
152 surface area). Both crustose (CCA) and articulated (branching) coralline algae (ACA) were
153 present. The field site has an eastern exposure, resulting in full morning sun and relatively early
154 shade in the evening. Foreshore locations of the pools resulted in daily emersion year-round
155 including during neap tides (mid-tide, approx. 5-6 m above chart datum). Pools emerged for 6-7 h
156 during low-tide periods. During that time, pools were completely separated from the adjacent open
157 water and their depths were effectively constant in winter (low-evaporation season), an indication
158 that there was no seawater leakage.

159 The volume of each of the five pools (from 16 to 39 L; **Fig. 2**) was estimated in April 2021
160 at the end of the emersion period just before high-tide flooding, by measuring salinity changes
161 when a known volume of freshwater was added and well mixed. To estimate the pools' initial
162 volumes, we also took into consideration the measured salinity changes throughout the emersion



163 period to estimate evaporative losses and combined this with the volume directly lost through
164 water sampling (see below). The pool projected area and the relative area covered by each type of
165 algae were estimated from aerial photographs, with a scale and analyzed using ImageJ (U. S.
166 National Institutes of Health, Bethesda, Maryland, USA, <https://imagej.nih.gov/ij>). Pool area
167 ranged from 0.3 to 0.6 m² (**Fig. 2**). The pools had slightly different community composition with
168 dominant calcifying red algae represented by *Lithophyllum incrustans* (CCA: 30 to 71 % of the
169 benthic cover) and *Ellisolandia elongata* (ACA: 0 to 6 % of the benthic cover). The remaining
170 pool area was either free of algal cover with only bare granitic rock visible or covered by soft
171 macroalgae. In summer (September 2020 and 2021), the pools also hosted the green algae *Ulva*
172 *sp.* and *Enteromorpha sp.* (2 to 44 % of the benthic cover: see **Supp. Mat. Pools: Fig. SP1-2**, for
173 results detailed by season) and, in Pool E, small single branches of the brown algae *Sargassum*
174 *muticum*, covering less than 0.5 % of the pool. We also noted the presence of diverse heterotrophs
175 such as anemones, sea sponges, small gobies, and shrimps. Calcifying invertebrates were
176 represented by four gastropod species: *Phorcus lineatus*, *Patella ulyssiponensis*, *Patella vulgata*
177 and *Gibbula pennanti*.

178 **Study design and seawater manipulation**

179 Fieldwork was conducted during the low-tide emersion periods, day and night. We refer to the
180 period from the beginning to the end of the pool emersion as a “low-tide emersion period” and to
181 each seasonal sampling period as a “field session” (**Table 1**). We sampled during three seasons:
182 winter (February 2020 and 2021), spring (April 2021), and summer (September 2020 and 2021).
183 During each field session, all the pools experienced both “future” (approximately year 2100 under
184 high emissions) and present-day (“present”, non-manipulated control) initial carbonate chemistry
185 conditions. During each low-tide emersion period (n = 23), we randomly selected two or three
186 pools in which we decreased pH to 7.5 at the start of the emersion. The following low-tide
187 emersion period, this was reversed and pools that had been subject to present-day conditions in the
188 previous low-tide emersion period were subject to future conditions and *vice versa*. However, due
189 to diverse constraints, in two of the 23 emersion periods all the pools were left under present-day
190 conditions.

191 **Table 1: Sampling schedule:** The dates of each field session are presented. Pools were monitored
192 throughout multiple low-tide emersion periods (diurnal and nocturnal).



| Season | Dates | Low-tide emersion periods (N) | |
|--------|---------------------|-------------------------------|-----------|
| | | Diurnal | Nocturnal |
| Winter | 14-17 February 2020 | 2 | 0 |
| | 9-19 February 2021 | 8 | 2 |
| Spring | 28-29 April 2021 | 2 | 0 |
| Summer | 2-11 September 2020 | 5 | 1 |
| | 6-9 September 2021 | 0 | 3 |

193

194 In this experiment, we compared "present" and "future" seawater carbonate chemistry
195 conditions. To simulate "future" carbonate chemistry conditions, we added small volumes of CO₂-
196 enriched seawater (total of ~100-200 mL) at the start of the emersion period in 50 mL increments
197 until the well-mixed pool water reached the desired pH levels (pH = 7.6, reached in less than 10
198 min.). CO₂-enriched seawater was prepared by super-saturating adjacent seawater in CO₂ using a
199 high-pressure CO₂ cylinder.

200 **Sampling and measurement of seawater parameters**

201 **Temperature, salinity, pH, oxygen, and ammonium:** From the start of the emersion period, we
202 measured five parameters periodically using HACH-Lange (Loveland, USA) probes: temperature,
203 pH_T (IntelliCAL PHC101, accuracy: ± 0.02 pH units), salinity (conductivity probe IntelliCAL
204 CDC401, ± 0.1 units), oxygen concentration (optical sensor IntelliCAL LDO101, accuracy: ± 0.1
205 mg L⁻¹ for 0 to 8 mg L⁻¹ ± 0.2 mg L⁻¹ for greater than 8 mg L⁻¹, maximum 22 mg L⁻¹) and NH₄⁺
206 concentration (ion selective electrode IntelliCAL ISENH4181, range: 0.018 - 9000 mg L⁻¹ NH₄⁺-
207 N). Pools were well-mixed before any measurement to assure no influence of gradients forming in
208 the pools. The measurement frequency during the emersion periods was every 15-20 min during
209 the day (n = 1392) and reduced to once an hour at night (n = 159), when temperature, pH and light
210 variations were limited or absent. pH was calibrated on the total scale (pH_T) using TRIS (2-amino-
211 2-hydroxy-1,3-propanediol) and AMP (2-aminopyridine) buffer solution with a salinity of 35.0,
212 following the recommendations from (Dickson et al., 2007).

213 **Total alkalinity:** Discrete samples for total alkalinity (TA) analysis were collected hourly. The
214 average time between two samples was 1.0 ± 0.2 hours (n = 492, median = 1.0) during daytime



215 and 1.4 ± 0.9 hours ($n = 135$, median = 1.0) during nighttime. Seawater (150 mL) was filtered with
216 $0.7 \mu\text{m}$ GF/F borosilicates filters directly after sampling. These samples were stored in a dark cool
217 box until the end of the tide (max. 7 h). Upon return to the lab, they were stored at 4°C in the dark
218 until they were either analyzed within the week or poisoned with $50 \mu\text{L}$ of saturated HgCl_2 (see
219 "*sample processing*"). TA was assessed potentiometrically using 50.0 ± 0.5 g of seawater and a
220 semi-automated titration system (0.1 M HCl, Titrino 848 plus by Metrohm, Switzerland; electrode
221 calibrated on the National Bureau of Standards scale). TA was determined using Gran titration
222 (Gran, 1952) according to the method of Haraldsson et al. (1997) and verified against reference
223 standards provided by A. Dickson (Scripps Institute of Oceanography, University of South
224 California, San Diego, United States). TA samples were analyzed with single ($n = 312$) or duplicate
225 ($n = 320$) measurements (the median of the standard deviation between duplicates was $1.05 \mu\text{mol}$
226 kg^{-1}). TA was salinity-normalized before further calculations, to take into account possible dilution
227 from rain or concentration from evaporation.

228 To take into account the influence of the changes in nutrients (NO_3^- , NO_2^- , PO_4^{3-} and NH_4^+)
229 on the changes in TA (Gazeau et al., 2015), we sampled seawater for nutrients in winter (February
230 2020) and summer (September 2020). Samples were taken during the day at the start and end of
231 the emersion periods in the five pools. Around 60 mL of seawater was immediately filtered on 0.2
232 μm cellulose filters, stored in 125 mL polyethylene bottles in a cool dark box (max. 7h), and then
233 frozen at -20°C until analysis. Nutrient concentrations were obtained using an AA3 auto-analyzer
234 (Seal Analytical) using the method from Aminot & K erouel (2007). Changes in nutrient
235 concentrations were near-negligible contributions to TA changes throughout a low-tide emersion
236 period ($< 6 \mu\text{mol kg}^{-1}$ i.e., $< 2\%$ of the observed change in TA, see full details in **Supp. Mat.**
237 **Nutrients**) and thus are ignored here.

238 **Light measurements:** Surface irradiance (photosynthetically active radiation, PAR) was
239 continuously recorded (every minute) during experiments at the field station, using a Li-Cor flat
240 quantum light sensor (LI-190R) and logger (LI-1500, LI-COR, Germany).

241 **Adjacent waters:** Temperature, salinity, pH and TA ($n = 5$) were similarly sampled and measured
242 at the sampling site during ebb tide, for the three seasons.

243 **Carbonate chemistry calculations**



244 The carbonate system parameters (e.g., $p\text{CO}_2$, DIC concentration, CO_3^{2-} concentration, and Ω_a , the
245 aragonite saturation state) were calculated from the measurements of pH_T , TA, temperature and
246 salinity using the R package *seacarb* (Gattuso et al., 2021) with the default dissociation constants
247 recommended by Dickson et al. (2007), except for the low temperatures encountered in February
248 2021 where the refined constants of Sulpis et al. (2020) were used. When salinity decreased by
249 more than 1.5 units per hour, data were excluded to avoid rain effects in the present study. When
250 calculated DIC and Ω_a were negative, likely due to inaccuracies in the measurement and
251 computation of the carbonate system, values were approximated to be 0 (7/627 values).

252 **Biological activity calculations**

253 The rates of Net Community Calcification (NCC; $\text{mmol CaCO}_3 \text{ m}^{-2} \text{ h}^{-1}$) and Net
254 Community Production (NCP) or Community Respiration (CR; $\text{mmol O}_2 \text{ m}^{-2} \text{ h}^{-1}$ or mmol C m^{-2}
255 h^{-1}) were calculated between two consecutive sampling times. These rates respectively represent
256 the measured changes of net CaCO_3 precipitation and net organic carbon production (or oxygen
257 consumption) by the community. Positive NCC represents net CaCO_3 precipitation (gross
258 precipitation > dissolution) and negative rates represent net dissolution (dissolution >
259 precipitation). NCP is positive when the community primary production exceeds respiration and
260 negative when community primary production is less than respiration. We use CR (not NCP) for
261 nights, when there is no primary production (oxygen consumption and carbon release only).

262 NCC was calculated using the alkalinity anomaly method (Smith & Key, 1975). Briefly,
263 for each mol of CaCO_3 precipitated, two moles of HCO_3^- combine with Ca^{2+} , and TA decreases
264 by two moles (*Eq. 1*). Two independent estimates of NCP (or CR) were calculated, one derived
265 from changes in ΔO_2 (NCP_{O_2} or CR_{O_2}) and one derived from ΔDIC and NCC (NCP_{DIC} or CR_{DIC}).

266 NCC and NCP (or CR) were thus calculated as follows:

$$267 \quad \text{NCC} = \frac{\Delta\text{TA}}{2\Delta t} \times \frac{V}{S} \quad (1)$$

$$268 \quad \text{NCP (or CR)}_{\text{O}_2} = \frac{\Delta\text{O}_2}{\Delta t} \times \frac{V}{S} \quad (2)$$

$$269 \quad \text{NCP (or CR)}_{\text{DIC}} = \frac{-\Delta\text{DIC}}{\Delta t} \times \frac{V}{S} - \text{NCC} \quad (3)$$



270 with ΔTA (mmol L^{-1}), ΔDIC (mmol L^{-1}) and ΔO_2 (mmol L^{-1}) the change in concentration of TA,
271 DIC and O_2 , between consecutive samples and Δt the duration between consecutive samples (h),
272 V pool volume (L), S the pool surface area (m^2).

273 Up to seven NCC and NCP (or CR) rates were calculated for each pool during each
274 emersion period (one per hour). These rates were used to investigate the direct correlation between
275 biological activity and environmental factors such as light intensity or Ω_a .

276 Rates calculated this way are however not independent from each other (i.e., the rate
277 measured at $t+2$ is dependent on the rate at $t+1$), limiting further statistical analyses on the effect
278 of the treatment. This is why, to investigate the effect of pH treatment (“present” vs. “future”) on
279 community biological activity, we also calculated NCC and NCP or CR using linear regressions
280 (NCC_{lm} and NCP_{lm} or CR_{lm}) between TA, [DIC] and [O_2] and time after the start of the emersion
281 period (for detailed results of the regressions, e.g., goodness-of-fit, see **Supp. Mat. LM1-3**). The
282 few data from diurnal tides that were taken after sunset were excluded from these regressions. For
283 oxygen, data was limited to the first three hours of emersion as high O_2 concentrations ($>22 \text{ mg L}^{-1}$)
284 and supersaturation ($>200 \%$) led to inaccurate measurements and/or possible oxygen degassing
285 afterwards (see **Supp. Mat. LM2**). This regression approach provides a single estimate of the rate
286 of NCC, NCP_{DIC} (or CR_{DIC}) and NCP_{O_2} (or CR_{O_2}) for each pool during each emersion period ($n =$
287 17 diurnal and 6 nocturnal low-tide emersion periods \times 5 pools = 115). These rates were then used
288 in generalized linear mixed models (GLMM) to assess the effect of pH treatment on diurnal and
289 nocturnal biological activity (see “*statistical analyses*” below).

290 We calculated community calcification and production budgets (respectively CCB and
291 CPB) at emersion as an indication of the night/day balance in calcification and production: when
292 CCB/CPB is positive the pool community calcifies/produces more by day than they
293 dissolve/respire at night. Both were calculated for winter (February 2020 and 2021) and summer
294 (September 2020 and 2021) for each pool as follows:

$$295 \quad \text{CCB} = \text{NCC}_D + \text{NCC}_N \quad (4)$$

$$296 \quad \text{CPB} = \text{NCP}_D + \text{CR}_N \quad (5)$$



297 with NCC_D and NCP_D (> 0) the average diurnal NCC and NCP for a given pool for a treatment
298 and a season and NCC_N and CR_N (< 0) the average nocturnal NCC and dark respiration for the
299 same conditions. Three approaches were used for estimating CPB, given the uncertainties of each
300 NCP estimate (see discussion): (1) O_2 -derived estimates of NCP (CPB_{O_2}), (2) DIC- derived
301 estimates (CPB_{DIC}) and (3) a “mixed” approach that combined nocturnal CR_{O_2} and diurnal NCP_{DIC}
302 (CPB_m), under the assumption that one mol of carbon is produced/consumed when one mol of O_2
303 is produced/consumed. Although CPB resemble gross community production in the way the rates
304 are calculated (difference between light and dark net production/respiration rates), if one wanted
305 to reuse these rates for gross community production, they should be do so with care due to
306 differences in night and day temperature (see extended discussion on this subject in Bracken et al.,
307 2022). The treatment effect was assessed on CCB and CPB by comparing the change due to the
308 “future” treatment in each pool.

309

310 **Statistical analyses**

311 All data are presented as mean \pm standard deviation (SD). The analyses were made using the
312 software R (R Core Team, 2017). The level of significance used was 5%. Because data were
313 measured on the same five pools but on different days for different treatments, we used GLMM to
314 test for the effect of treatment on NCC_{lm} and on O_2 and DIC-derived NCP_{lm} (or CR_{lm}), assigning
315 sampling days (i.e., low-tide emersion periods) as the random factor and pools (five levels), mean
316 temperature of the pool during low-tide emersion period (a continuous proxy for season) and
317 treatment (*Treat*: “future” vs. “present”) as fixed factors. This was performed using the R package
318 *nlme* (Pinheiro et al., 2018). Models with and without standardized residuals were compared using
319 ANOVAs and, when different, Akaike Information Criteria (AIC) was used to choose the best
320 fitted-model of the two. For GLMM, mean daily PAR was not used as it has strong collinearity
321 with mean daily temperature/season. We used ANOVAs to test the effect of temperature, pool and
322 treatment on initial (averaged over the first hour of emersion) and final (averaged for > 5 hours
323 after emersion) carbonate chemistry conditions. The normality of the data was tested using
324 Shapiro–Wilk tests and qq-plots, while variance homogeneity was tested with Bartlett tests.

325



326 RESULTS

327 1/ Environmental conditions

328 **Adjacent waters:** Temperatures (and salinity) measured in the seawater adjacent to the pools were
329 6-7°C in winter (February; salinity $S=35.0$), 11-12°C in spring (April; $S=35.5$) and 17-18°C in
330 summer (September; $S=36.0$). This seawater was characterized by average pH_T of 8.01 ± 0.06
331 units, total alkalinity of $2319 \pm 6 \mu\text{mol kg}^{-1}$, $p\text{CO}_2$ of $445 \pm 69 \mu\text{atm}$, $\Omega_a = 2.2 \pm 0.3$ and $[\text{O}_2] =$
332 $100 \pm 1 \%$ of air saturation (or $10.1 \pm 1.5 \text{ mg L}^{-1}$; $n=5$).

333 **Light duration and intensity:** In Roscoff, day:night periods are typically 10h:14h in February,
334 14h:10h in April and September. Photosynthetically active radiation (PAR) was two to three times
335 higher in spring/summer (**Fig. 3A**: April/September $\sim 1500 \mu\text{mol m}^{-2} \text{ s}^{-1}$) than in winter (February
336 $\sim 500 \mu\text{mol m}^{-2} \text{ s}^{-1}$).

337 **Carbonate chemistry conditions at the start of the emersion period (< 1h post emersion):**
338 Both for diurnal and nocturnal tides, the initial pH was significantly lower in pools with added
339 CO_2 than in the present-day pools (Day: $pH_T = 8.2 \pm 0.1$ vs. 7.5 ± 0.2 units; Night: 8.0 ± 0.1 vs.
340 7.4 ± 0.1 units for “present” and “future” pools respectively; *Treat* $p < 0.001$; detailed results in
341 **Fig. S2-3, Table S1-2**). This corresponds to $p\text{CO}_2$ of 260 ± 100 vs. $1900 \pm 835 \mu\text{atm}$ (day) and
342 510 ± 90 vs. $2310 \pm 410 \mu\text{atm}$ (night) for pools in “present” and “future” conditions respectively.
343 Adding CO_2 in the pools increased the mean DIC concentration by $320 \mu\text{mol kg}^{-1}$ during the day
344 and $240 \mu\text{mol kg}^{-1}$ during the night. In “present-day” conditions, the pools started at supersaturated
345 levels with regards to aragonite (day: $\Omega_a = 3.3 \pm 1.3$, night: 2.2 ± 0.3). Adding CO_2 significantly
346 decreased Ω_a (*Treat*: $p < 0.001$, **Table S1**) leading to initial “future” conditions often
347 undersaturated with regards to aragonite ($\Omega_a = 0.8 \pm 0.5$) by day and always undersaturated
348 conditions by night ($\Omega_a = 0.6 \pm 0.1$). Furthermore, in “future” diurnal conditions, pools were
349 always undersaturated with respect to aragonite from the start of the emersion period in February
350 ($\Omega_a = 0.5 \pm 0.2$) but not in April ($\Omega_a = 1.1 \pm 0.7$) and September ($\Omega_a = 1.2 \pm 0.5$; **Table S1**). At the
351 start of emersion, total alkalinity was $2303 \pm 34 \mu\text{mol kg}^{-1}$ (similar to adjacent seawater), and
352 uncorrelated with treatment ($p > 0.05$) and temperature ($p > 0.6$).

353 As data was averaged on the first hour post-emersion, the mean initial oxygen
354 concentration calculated was already affected by NCP by day ($14.0 \pm 2 \text{ mg O}_2 \text{ L}^{-1}$) and CR by



355 night ($9.5 \pm 1.5 \text{ mg O}_2 \text{ L}^{-1}$; vs. $10.1 \pm 1.5 \text{ mg O}_2 \text{ L}^{-1}$ for adjacent seawater). This was also visible
356 in CO_2 partial pressure, with lower $p\text{CO}_2$ than expected during the first hour post-emersion by day
357 ($262 \pm 102 \text{ } \mu\text{atm}$ vs. $445 \pm 69 \text{ } \mu\text{atm}$ for adjacent seawater) and higher $p\text{CO}_2$ at night (508 ± 88
358 μatm) in the “present-day” conditions.

359 2/ Diurnal tides

360 **Diurnal pool chemistry:** Starting from the aforementioned values at emersion, the pools followed
361 a clear temporal evolution due to solar irradiance and community metabolism (**Fig. 3**). Firstly, we
362 observed increases in salinity (+1.5 units on average, **Fig. 3A**) and temperature (+4°C in
363 September, +6°C in April on average) in summer and spring. In winter, temperatures tended to
364 decrease (-1.7°C on average) with air temperatures colder than that of the seawater; salinity was
365 stable (35.5 ± 0.8).

366 Secondly, we observed positive NCP corroborated by a doubling in oxygen concentration
367 (**Fig. 3A**) a few hours after the start of emersion. In parallel, the seawater DIC concentration
368 decreased by half from the initial concentration (from 2130 ± 195 to $1140 \pm 560 \text{ } \mu\text{mol kg}^{-1}$; **Fig.**
369 **3B**), the range of which largely depended on the season (**Fig. S2**). For instance, in February, DIC
370 consumption in pool seawater averaged $\sim 700 \text{ } \mu\text{mol kg}^{-1}$ over a low-tide period, while it averaged
371 $\sim 1500 \text{ } \mu\text{mol kg}^{-1}$ in September. Particularly extreme conditions, with DIC concentrations
372 effectively reaching $0 \text{ } \mu\text{mol kg}^{-1}$, were observed in two of the pools, at three tides in September
373 2020 (see further details below in “5/ *The particular case of September 2020 tides*”). At the end
374 of diurnal emersions, average $p\text{CO}_2$ was always below $100 \text{ } \mu\text{atm}$, reaching as low as $1 \pm 2 \text{ } \mu\text{atm}$
375 in September (**Fig. 3B, Table S1**). As a result, diurnal pH_T increased to 9.1 ± 0.6 by the end of
376 emersion, with maximum values up to 10.3 in summer (**Fig. 3B**). At the end of a diurnal emersion
377 period, the pools’ pH was stable, reaching either a plateau or decreasing after sunset (see PAR in
378 **Fig. 3A**). Similarly, at the end of diurnal emersion periods, Ω_a was high (5.6 ± 3.0 on average;
379 max 10.4). Lastly, we observed a diurnal decrease in TA by $415 \text{ } \mu\text{mol kg}^{-1}$ on average, indicative
380 of net calcification.

381 It is noteworthy that the carbonate chemistry conditions experienced at the end of diurnal
382 emersion converged whatever the initial treatment (**Fig. S2, Table S1**). For instance, while Ω_a was
383 significantly different between treatments at the start of the emersion period, both treatments



384 reached similar Ω_a at the end of emersion (> 5 h) of around 5.3 ± 2.2 (ANOVA: Treat: $p = 0.1$,
385 Temp: $p = 0.002$, Pool: $p = 0.01$). There was less convergence for pH_T where, even five hours after
386 emersion, there were still statistically significant, albeit small, differences between treatments (p
387 < 0.001 for pH_T with 9.2 ± 0.6 for “present” and 9.0 ± 0.6 for “future” pools).

388 **Diurnal biological activity:** Net community production was positive during daytime, except at
389 sunset (Fig. 3C). NCP was significantly correlated to light intensity (PAR) and further results for
390 hourly NCP and their correlation to hourly averaged PAR, Ω_a and temperature can be found in the
391 **Supp. Mat. (Fig. S5 and S6).**

392 As expected, seasons/temperature affected net oxygen production (O_2 -derived NCP_{lm}),
393 increasing from 7 ± 3 $\text{mmol O}_2 \text{ m}^{-2} \text{ hr}^{-1}$ in February to 18 ± 11 $\text{mmol O}_2 \text{ m}^{-2} \text{ hr}^{-1}$ in September
394 (Fig. 4A and Table 2A: GLMM, $p < 0.001$). CO_2 addition increased O_2 -derived NCP_{lm} by 20%,
395 from 10 ± 7 $\text{mmol O}_2 \text{ m}^{-2} \text{ hr}^{-1}$ in “present” conditions to 12 ± 9 $\text{mmol O}_2 \text{ m}^{-2} \text{ hr}^{-1}$ ($p = 0.0015$). Net
396 oxygen production differed across pools ($p < 0.003$), with significantly more productivity in pool
397 C (17.6 ± 12.7 $\text{mmol O}_2 \text{ m}^{-2} \text{ hr}^{-1}$) and D (10.6 ± 5.6 $\text{mmol O}_2 \text{ m}^{-2} \text{ hr}^{-1}$), compared to the pools A,
398 B and E (8.1 ± 4.1 $\text{mmol O}_2 \text{ m}^{-2} \text{ hr}^{-1}$).

399 Results are similar for DIC-derived NCP_{lm} (Fig. 4A and Table 2B), with primary
400 production ranging from 6 ± 2 $\text{mmol C m}^{-2} \text{ hr}^{-1}$ in February up to 12 ± 5 $\text{mmol C m}^{-2} \text{ hr}^{-1}$ in
401 September ($p < 0.001$). As for O_2 -derived NCP_{lm} CO_2 addition increased DIC-derived NCP_{lm} by
402 20 % ($p < 0.001$, Fig. 4A). This increase was particularly apparent in the summer, where NCP_{lm}
403 increased from 11 ± 4 $\text{mmol m}^{-2} \text{ hr}^{-1}$ in the “present” treatment to 15 ± 5 $\text{mmol C m}^{-2} \text{ hr}^{-1}$ in the
404 “future” treatment (+ 35 %). Compared to pool A, productivity was significantly lower in pools B
405 and E and significantly higher in pools C and D ($p < 0.003$).

406 By day, with the exception of sunset, net community calcification was positive (NCC and
407 $\text{NCC}_{\text{lm}} > 0$: Fig. 3C and 4B) and occurred in an environment that was supersaturated with regards
408 to aragonite (Fig. 3B). This was with the exception of a few emersion periods in September 2020
409 where dissolution was observed despite high saturation state conditions (further details below).
410 Similar to NCP_{lm} , diurnal net calcification rates (NCC_{lm}) were strongly influenced by
411 temperature/season (Fig. 4B and Table 2C: GLMM, $p < 0.001$) ranging from 1.2 ± 0.5 mmol
412 $\text{CaCO}_3 \text{ m}^{-2} \text{ hr}^{-1}$ in February to 3.3 ± 1.3 $\text{mmol CaCO}_3 \text{ m}^{-2} \text{ hr}^{-1}$ in September. NCC hourly rates



413 positively correlated with averaged Ω_a ($p < 0.0001$; $NCC = 0.15 \times \Omega_a + 0.85$; linear regression
 414 presented in **Fig. S6**), significantly but not strongly ($R^2 = 10\%$). CO_2 addition did not influence
 415 NCC_{lm} rates during the day ($p = 0.47$). However, NCC_{lm} did differ across pools ($p < 0.003$): rates
 416 were relatively low in pool E – lowest CCA cover (30%) – ($1.4 \pm 1.4 \text{ mmol CaCO}_3 \text{ m}^{-2} \text{ hr}^{-1}$), and
 417 high in pool D – highest CCA cover (70%) – ($2.2 \pm 0.8 \text{ mmol CaCO}_3 \text{ m}^{-2} \text{ hr}^{-1}$) compared to the
 418 three other pools ($2.0 \pm 1.25 \text{ mmol CaCO}_3 \text{ m}^{-2} \text{ hr}^{-1}$).

419 **Table 2: Results of the generalized linear mixed-effect models for A) O_2 -derived NCP_{lm}**
 420 **($\text{mmol O}_2 \text{ m}^{-2} \text{ hr}^{-1}$), B) DIC-derived NCP_{lm} ($\text{mmol C m}^{-2} \text{ hr}^{-1}$) and C) NCC_{lm} ($\text{mmol CaCO}_3 \text{ m}^{-2}$**
 421 **hr^{-1}) during the day and night.** The models include three fixed factors: *Temp* (mean temperature:
 422 a continuous factor), *Treat* (for CO_2 “future” treatment vs. “present”, two levels) and *pools* (vs. A,
 423 five levels), and one random effect (*low-tide emersion period* or the calendar day at which the pool
 424 was measured). Significant *p*-values are highlighted in bold.

425

| A. | O_2 -derived NCP_{lm} | Estimate | Standard Error | <i>p</i> -value | |
|-------|---------------------------|---------------------------------|---------------------|-----------------|-------------------|
| Day | Intercept | 1.49 | 1.37 | 0.28 | |
| | Fixed Effects | <i>Temp</i> | 0.54 | 0.13 | <0.001* |
| | | <i>Treat</i> | 1.09 | 0.33 | 0.0015* |
| | | <i>Pools</i> | A, B, E \neq C, D | | <0.003* |
| | Random Effect | <i>Low-tide emersion period</i> | 8.90 | 0.90 | <0.001* |
| Night | Intercept | 2.87 | 0.98 | 0.005* | |
| | Fixed Effects | <i>Temp</i> | -0.43 | 0.06 | <0.001* |
| | | <i>Treat</i> | -0.25 | 0.28 | 0.39 |
| | | <i>Pools</i> | A, B, D \neq C, E | | <0.03* |
| | Random Effect | <i>Low-tide emersion period</i> | -3.46 | 0.87 | <0.001* |

426

427



| B. | | DIC-derived NCP _{lm} | Estimate | Standard Error | p-value |
|-------|----------------------|---------------------------------|----------------|----------------|-------------------|
| Day | Intercept | | 2.3 | 1.08 | 0.035* |
| | Fixed Effects | <i>Temp</i> | 0.38 | 0.08 | <0.001* |
| | | <i>Treat</i> | 1.25 | 0.25 | <0.001* |
| | | <i>Pools</i> | A ≠ B, C, D, E | | <0.003* |
| | Random Effect | <i>Low-tide emersion period</i> | 7.7 | 0.7 | <0.001* |
| Night | Intercept | | -0.94 | 1.4 | 0.51 |
| | Fixed Effects | <i>Temp</i> | -0.92 | 0.19 | 0.053 |
| | | <i>Treat</i> | -0.25 | 0.28 | <0.001* |
| | | <i>Pools</i> | A, B, D, E ≠ C | | 0.016* |
| | Random Effect | <i>Low-tide emersion period</i> | 1.61 | 0.57 | 0.01* |

428

| C. | | NCC _{lm} | Estimate | Standard Error | p-value |
|-------|----------------------|---------------------------------|----------------|----------------|-------------------|
| Day | Intercept | | -0.16 | 0.31 | 0.61 |
| | Fixed Effects | <i>Temp</i> | -0.13 | 0.02 | <0.001* |
| | | <i>Treat</i> | 0.06 | 0.08 | 0.47 |
| | | <i>Pools</i> | A, B, C ≠ D, E | | <0.003* |
| | Random Effect | <i>Low-tide emersion period</i> | -1.90 | 0.24 | <0.001* |
| Night | Intercept | | 0.64 | 0.26 | 0.026* |
| | Fixed Effects | <i>Temp</i> | 0.009 | 0.016 | 0.57 |
| | | <i>Treat</i> | 0.28 | 0.07 | 0.0017* |
| | | <i>Pools</i> | A, B, C ≠ D, E | | <0.017* |
| | Random Effect | <i>Low-tide emersion period</i> | 0.83 | 0.078 | <0.001* |

429



430 **3/ Nocturnal tides**

431 **Nocturnal pool chemistry:** Seawater temperatures during the nights were stable (**Fig. 3A**)
432 throughout the emersion period in summer (from $17.3 \pm 0.4^\circ\text{C}$ < 1 h post-emersion to $17.2 \pm 0.2^\circ\text{C}$
433 > 5 h post-emersion) and winter (from $8.4 \pm 1.4^\circ\text{C}$ to $7.8 \pm 2.7^\circ\text{C}$ in February; no April nights).
434 We highlight the wide range of winter seawater temperatures with an exceptionally cold tidal cycle
435 (5°C on the 13th of February 2021) due to air temperatures of $3\text{--}4^\circ\text{C}$ (observations from the Île de
436 Batz meteorological station). There was a decline in salinity at night in some winter emersion
437 periods (**Fig. 3A**), due to high air humidity and/or rain. Data where salinity dropped by more than
438 1.5 units in less than an hour were removed from further analyses on net community calcification
439 and respiration.

440 After five hours of emersion, O_2 concentration had decreased by half (from $\approx 10 \text{ mg O}_2 \text{ L}^{-1}$
441 to $4.9 \pm 3.3 \text{ mg O}_2 \text{ L}^{-1}$) (**Fig. 3A**) due to community respiration. Simultaneously, pH_T decreased
442 to 7.6 ± 0.2 (“present”) or stayed at 7.4 ± 0.2 (“future”; **Fig. 3B and S2, Table S1**), with significant
443 effects of pools, treatment and temperature ($p < 0.001$ for all three). DIC concentration increased
444 by $+256 \mu\text{mol kg}^{-1}$ on average over an emersion period. The range of this increase depended on
445 the temperature and the pool: in winter ($5\text{--}10^\circ\text{C}$), present-day pool seawater gained $+130 \mu\text{mol kg}^{-1}$
446 ($+60$ for “future” pools) of DIC over an emersion period, when in summer they gained $+370$
447 $\mu\text{mol kg}^{-1}$ for “present” (“future”: $+310 \mu\text{mol kg}^{-1}$) pools. Saturation state converged towards
448 similar undersaturated levels at night (**Fig. 3B and S2, Table S1**): Ω_a stayed stable in the “future”
449 treatment (0.7 ± 0.2 units on average) and decreased in the “present-day” treatment (-1.2 units
450 from initial Ω_a). At the end of nocturnal emersion Ω_a were still statistically different due to the
451 initial treatment ($p < 0.001$ for *Treat*, *Temp* and *Pools*).

452 **Nocturnal biological activity:** At night, oxygen was consumed, i.e., we observed dark respiration
453 (CR; **Fig. 3C**). Community respiration (O_2 -derived CR_{lm}) varied according to season (**Fig. 4A** and
454 **Table 2A**: $p < 0.001$): temperature linearly increased nocturnal respiration rates from -1.0 ± 1.2
455 $\text{mmol O}_2 \text{ m}^{-2} \text{ hr}^{-1}$ in February to $-4.7 \pm 1.3 \text{ mmol O}_2 \text{ m}^{-2} \text{ hr}^{-1}$ in September. The CO_2 treatment did
456 not influence night respiration ($p = 0.39$). Respiration rates were significantly influenced by pools
457 ($p = 0.03$), probably linked to the relative biomass of heterotrophs and autotrophs; respiration was
458 significantly higher in pool C ($-4.6 \pm 2.8 \text{ mmol O}_2 \text{ m}^{-2} \text{ hr}^{-1}$) and significantly lower in pool E (-2.4
459 $\pm 1.4 \text{ mmol O}_2 \text{ m}^{-2} \text{ hr}^{-1}$) than in pools A, B and D ($-3.4 \pm 2.1 \text{ mmol O}_2 \text{ m}^{-2} \text{ hr}^{-1}$).



460 Night respiration estimated using DIC and NCC was near zero ($CR_{lm} = -0.2 \pm 0.7 \text{ mmol m}^{-2}$
461 hr^{-1}). At these low rates, uncertainties associated with much higher rates of net dissolution
462 (negative NCC) sometimes led to spuriously positive DIC-derived CR estimates, hindering
463 interpretation. Nevertheless, DIC-derived community respiration was ten times lower in February
464 than in September (-0.2 ± 0.7 and $-2.3 \pm 1.1 \text{ mmol C m}^{-2} \text{ hr}^{-1}$ respectively), although it was not
465 linearly driven by temperature ($p = 0.053$; **Fig. 4B** and **Table 2B**). Adding CO_2 to the pools
466 influenced DIC-derived community respiration in a way that was inverse to that seen with O_2 , but
467 as stated above, this was likely an artifact of subtracting NCC from small DIC changes. As for O_2 ,
468 DIC-derived CR_{lm} significantly changed depending on the pools.

469 At night, the pools experienced significant net community dissolution ($NCC < 0$; **Fig. 3C**)
470 even when waters were supersaturated with regards to aragonite in the “present” treatment (**Fig.**
471 **3B**: $\Omega_a > 1$). Nocturnal net dissolution rates (NCC_{lm}) were not significantly affected by temperature
472 in the range investigated ($5\text{--}18^\circ\text{C}$; **Fig. 4C** and **Table 2C**: $p = 0.57$). However, adding CO_2 in the
473 pools increased net dissolution rates ($p = 0.0017$) from $-0.7 \pm 0.3 \text{ mmol CaCO}_3 \text{ m}^{-2} \text{ hr}^{-1}$ to $-1.0 \pm$
474 $0.4 \text{ mmol CaCO}_3 \text{ m}^{-2} \text{ hr}^{-1}$ (+40 %). Similarly, looking instead at hourly rates (NCC), dissolution
475 correlated significantly ($p < 0.0001$) with Ω_a ($NCC = 0.34 \times \Omega_a - 1.22$; $R^2 = 11 \%$; **Fig. S6**). The
476 strength of this correlation depended on seasons and pools (**Fig. S7**). Net dissolution rates (NCC_{lm})
477 significantly differed by pool ($p < 0.0017$): the lowest rates were observed in pool E (-0.4 ± 0.2
478 $\text{mmol CaCO}_3 \text{ m}^{-2} \text{ hr}^{-1}$) – the pool with the lowest CCA cover –, and the highest dissolution in pool
479 D – the pool with the highest CCA cover (-1.0 ± 0.4 vs. $-0.9 \pm 0.3 \text{ mmol CaCO}_3 \text{ m}^{-2} \text{ hr}^{-1}$ for A, B
480 and C).

481

482 **4/ Influence of the treatment on CPB and CCB**

483 Pools fixed more carbon during the day than they respired at night, i.e., the community production
484 budget (CPB: balance between night and day) was positive in all the pools, both in winter and
485 summer and whatever the treatment (**Fig. 5**). CPB_{DIC} and CPB_m estimates were typically lower
486 than CPB_{O_2} (in 14/20 cases and 18/20 cases respectively). The production budget was significantly
487 lower in winter than in summer (FEB: $CPB_{O_2} = 3 \pm 1 \text{ mmol O}_2 \text{ m}^{-2} \text{ h}^{-1}$, SEP: $7 \pm 5 \text{ mmol O}_2 \text{ m}^{-2}$
488 h^{-1} ; t-test: $t = -2.4$, $df = 9.8$, $p = 0.03$). Adding CO_2 increased CPB in all the pools in summer by +
489 $3.0 \pm 2.1 \text{ mmol O}_2 \text{ m}^{-2} \text{ h}^{-1}$, an increase in production by 50 to 80 % (ΔCPB ; **Fig. 5**). In winter, there



490 was no evidence of such a “fertilization effect” across the most accurate CPB estimates for this
491 season (CPB_{O2}, CPB_m): we only observed a significant increase in production due to CO₂ addition
492 in two of the pools (+60 % to +120 % for A and B). For the three other pools, CPB either induced
493 minimal changes (< 20 % for C and E) or a decrease in production (D: down to -34 %). DIC-
494 derived ΔCPB in winter (all positive) should be interpreted with caution since some nocturnal
495 CR_{lm} were spuriously positive in the “future” treatment (see “nocturnal biological activity” above).

496 The pools calcified more during the day than they dissolved at night (CCB > 0), both in
497 summer and winter (**Fig. 5**). CCB was significantly lower in winter than in summer (FEB: CCB =
498 0.2 ± 0.2 mmol CaCO₃ m⁻² h⁻¹, SEP: 1.2 ± 0.6 mmol CaCO₃ m⁻² h⁻¹; t-test: $t = -5.2$, $df = 11.7$, $p =$
499 0.0002). In winter, adding CO₂ decreased CCB by more than 80 % in pools C, D, and E (**Fig. 5**).
500 The CO₂ addition even resulted in a transition from a positive community calcification balance to
501 dissolution in pool C (133 % change, from +0.5 to -0.2 mmol CaCO₃ m⁻² h⁻¹). For the two other
502 pools (A and B), winter CO₂ addition increased their relatively small calcification balance (A: +87
503 %, from 0.1 to 0.2 mmol CaCO₃ m⁻² h⁻¹ and B: +71 %, from 0.2 to 0.3 mmol CaCO₃ m⁻² h⁻¹). In
504 summer, changes in CCB due to treatment appeared minimal in pools A, B and E (< 15 % change)
505 and either increased (C: +67%) or decreased (D: -57%) in the two other pools. In analyses not
506 presented here, when this budget takes into account winter night:day duration (14:10), all the
507 pools’ budgets switch to net dissolution in future conditions.

508

509 **5/ The particular case of September 2020 tides**

510 During diurnal tides of September 2020 (high PAR and high temperature summer conditions), we
511 observed an unexpected phenomenon: dissolution occurred at extremely high pH_T values (9-10)
512 in pools C and E (**Fig. 6**). Under these conditions effectively all the seawater DIC in these pools
513 was consumed by photosynthesis and calcification (DIC ≈ 0 mmol kg⁻¹) four hours after emersion.
514 As such, the CO₃²⁻ concentration was also effectively zero and the pools reached very low
515 saturations states (Ω_a ≈ 0) despite high pH (**Fig. 6**). These conditions were quickly followed by
516 indicators of CaCO₃ dissolution (increasing TA and DIC) instead of the expected diurnal
517 precipitation. It is therefore noteworthy that dissolution may happen at high pH, and that pH and



518 Ω can decorrelate (**Fig. 7**) in situations with high photosynthesis and limited mixing of water
519 masses.

520

521 **DISCUSSION**

522 Temperate tidal pools are environments of extreme variability. In our pools, we observed seawater
523 temperatures that could increase by up to 10°C in a few hours compared to the adjacent ocean.
524 During diurnal emersion periods, oxygen concentrations doubled and pH could increase to pH 10
525 in present-day summer conditions. At night, pH routinely reached levels usually used as the
526 “treatment” for ocean acidification perturbation experiments (~7.6). Organisms present in the tidal
527 pools may therefore already be adapted or acclimatized to extreme variability in pH and saturation
528 state, which could affect their responses to ocean acidification (Andersson et al., 2015). For
529 example, CCA from a site with naturally high $p\text{CO}_2$ variability calcified ~50 % more than
530 individuals from a nearby site of low variability when submitted to oscillating high $p\text{CO}_2$
531 treatments (Johnson et al., 2014). Here we show that, even in intertidal communities likely already
532 acclimated or adapted to variable conditions, with potentially large phenotypic plasticity,
533 acidification can still modify net community production and calcification rates.

534 **Diurnal fertilization under CO_2 addition**

535 Adding CO_2 to simulate future seawater acidification in the pools led to a diurnal fertilization
536 effect. This increase in the community’s net primary production by 20% was particularly visible
537 in summer (+ 35%), at higher temperatures/metabolic rates. Adding CO_2 , we also added substrate
538 for photosynthesis in the form of DIC (**Fig. 3B**) that the algae of the pools can assimilate,
539 potentially supporting higher DIC use and algal primary production. This effect was apparent from
540 the start of the emersion, suggesting a direct effect of increasing DIC concentration in the pools.
541 It seems that photosynthesis in the pools was carbon-limited and that carbon addition therefore
542 enhanced primary production, in winter and to an even greater extent in summer. During
543 photosynthesis, the uptake of inorganic carbon leads to a significant decrease in DIC - even in
544 present-day conditions. Intertidal algae are typically adapted to this with coralline algae in
545 particular containing CCMs (CO_2 concentrating mechanisms) that allow them to achieve primary
546 production in low DIC concentrations (Raven, 2011). Increasing seawater DIC may however



547 promote an increase in active and/or passive CO_2 and HCO_3^- fluxes towards photosynthetic
548 compartments. Borowitzka (1981) found that the photosynthetic rate of an intertidal CCA was
549 highest at pH 6.5 to 7.5 (increased from pH 8.1), a change in pH that was achieved using HCl,
550 suggesting that increased photosynthetic activity could also be linked to proton gradients/pumps
551 and/or decreased energy expenditure needed to operate CCMs rather than directly related to CO_2
552 gradients or higher substrate availability.

553 In winter and summer, pools in present-day and future conditions were autotrophic at
554 emersion ($\text{NCP}_D > \text{CR}_N$, **Fig. 5**). If we consider the CPB as integrated diurnal NCP and nocturnal
555 CR over 24 hours (assuming equal day:night duration), this means that the pools always fixed
556 more carbon during the day than they respired at night at emersion ($\text{NCP} \gg \text{CR}$), regardless of
557 treatment. One methodological uncertainty we highlight regarding net production is that diurnal
558 DIC-derived NCP estimations were 50 % higher than O_2 -derived NCP estimates (**Fig. 3C and Fig.**
559 **4**, $\text{NCP}_{\text{DIC}} = 1.6 \pm 0.05 \text{ NCP}_{\text{O}_2}$ by day; $R^2 = 75\%$). This discrepancy was far less apparent during
560 nights, when methods agreed on respiration rates ($\text{CR}_{\text{DIC}} = 1.0 \pm 0.09 \text{ CR}_{\text{O}_2}$; $R^2 = 56\%$). While
561 O_2 -derived NCP appears accurate during the night, O_2 production during the day is likely to have
562 been underestimated due to degassing (e.g., visible formation of oxygen bubbles at the surface of
563 algae, $>150\%$ air saturation by day vs. $<100\%$ at night). Thus, estimating diurnal net production
564 using oxygen measurements may not be appropriate in algae-dominated environments such as
565 these tidal pools. Nevertheless, despite the difference in absolute NCP estimates, both approaches
566 indicate a diurnal fertilization effect.

567

568 **Nocturnal dissolution under CO_2 addition**

569 In the present study, natural mesocosms - temperate coralline-dominated tidal pools - were used
570 to investigate the effect of ocean acidification on net calcification at the community level. As we
571 observed a fertilization effect of CO_2 addition by day, we could have expected that it would also
572 enhance diurnal calcification – as photosynthesis and calcification are tightly linked (Martin et al.,
573 2013; Martin et al., 2013; Williamson et al., 2017) -, but this was not observed. Treatment had no
574 significant effect on the daytime net calcification rates, and diurnal variability in calcification
575 appears to be predominately driven by PAR, temperature, and metabolic activity (NCP). Increasing
576 metabolic rates - in turn increasing calcification rates - may have however counterbalanced any
577 calcification suppression or increased dissolution due to acidification, making its effect invisible.



578 Noisette et al. (2013) similarly found no effect of $p\text{CO}_2$ treatment on light calcification for *E.*
579 *elongata*. However, the authors reported a significant decrease in light calcification in *L.*
580 *incrustans*, net calcification even switched to net dissolution in 750 and 1000 $\mu\text{atm } p\text{CO}_2$
581 treatments. While our “future” treatments started at $p\text{CO}_2$ levels higher than 1000 μatm , the fact
582 that CO_2 addition did not influence diurnal calcification could also be due to favorable saturation
583 state conditions in the micro-environment in which calcification occurs. The diffusive boundary
584 layer (DBL) can enhance CaCO_3 precipitation micro-environment conditions due to the uptake of
585 CO_2/DIC for photosynthesis. For instance, in light conditions, CCA surface pH has been shown to
586 reach as high as 8.6 (Houlihan et al., 2020) in surrounding seawater at pH 7.7 (+1.1 pH units),
587 which would be highly favorable to calcification. But more complex interactions may also be at
588 work, e.g., CCA may use increases in HCO_3^- (due to CO_2 dissolution) to calcify, making them
589 more resistant to ocean acidification, as suggested by Comeau et al. (2013).

590 There was net CaCO_3 dissolution in the pools at night ($-0.7 \text{ mmol CaCO}_3 \text{ m}^{-2} \text{ hr}^{-1}$), even
591 when waters were still supersaturated with regards to aragonite under present-day conditions.
592 Night dissolution may be a sign that the DBL of the calcifiers inhabiting the pools is
593 undersaturated, possibly as a result of respiration. Indeed, Houlihan et al. (2020) observed that
594 nocturnal algal respiration by CCA, increased CO_2 in the DBL, decreasing pH of the DBL by 0.1
595 units. Such a small pH decrease is however unlikely to explain alone an undersaturation of the
596 calcifying environment as aragonite saturation state was still above 1.2 in most of the “present-
597 day” conditions. However, given the solubility of high-Mg calcite - the mineral composing *L.*
598 *incrustans* and *E. elongata* in particular (Ries, 2011) - can be twice that of aragonite (Sulpis et al.,
599 2021; Yamamoto et al., 2012), it is possible that undersaturation already occurs at night for this
600 mineral even for $\Omega_a > 1$. Adding CO_2 (from 445 to 1500-2000 μatm) at the start of emersion
601 significantly increased net dissolution (NCC_{lm}), by 40 % in summer and 70 % in winter. In a
602 previous single-species experiment, Noisette et al. (2013) demonstrated that - for *L. incrustans*
603 from an area close to our site – dark dissolution doubled with increasing $p\text{CO}_2$ (1000 μatm vs. 380
604 μatm), unlike *E. elongata*, for which there was no effect of $p\text{CO}_2$: the ACA even calcified in the
605 dark up to 750 μatm (see also similar results from Egilsdottir et al., 2013). Since *L. incrustans* is
606 the major calcifying species of the tidal pools we studied, it is likely this species drives the results
607 we observed at the pool community scale. Regardless of the treatment, nocturnal net dissolution



608 rates (NCC) were also significantly correlated with Ω_a , results similar to those found by
609 Kwiatkowski et al. (2016) in temperate tidal pools of California, without CO₂ addition.

610 In summer, pools in present-day and future conditions were precipitative (CCB > 0),
611 meaning that diurnal net calcification exceeded nocturnal net dissolution, regardless of treatment.
612 Adding CO₂ in summer did not consistently change CCB, with most pools showing little change
613 in CCB due to treatment. By contrast, in the colder winter, the calcification budget was at least 50
614 % lower than in summer (“present”), with some pools that had comparable net calcification during
615 the day to net dissolution at night. During this season, adding CO₂ had variable impacts on CCB,
616 decreasing it in three of the pools by more than 80 % and increasing relatively small CCB in two.
617 These variable effects may be due to differences in community composition and highlight the
618 difficulty in generalizing the results of natural mesocosm manipulations in which the initial
619 community composition is not controlled. Nevertheless, we expected CO₂ addition to have a
620 greater negative effect in winter (more dissolution) than in summer, with saturation states being
621 lower due to colder temperatures, making it more of a “crucial”/ “bottleneck” season. This
622 emphasizes the need to study the effect of ocean acidification across seasons and temperature
623 ranges, especially given the associated changes in algal community composition and metabolic
624 activity.

625

626 **Instances of aragonite undersaturation at high pH**

627 An unexpected phenomenon happened in the pools C and E in summer: although we measured
628 very high pH values, we observed that total alkalinity suddenly increased, a sign of fast net
629 dissolution. When we then computed the carbonate chemistry, the saturation states were
630 surprisingly low ($\Omega_a = 0$ for $\text{pH}_T = 10$), which was due to near-zero DIC concentrations – and thus
631 near-zero CO₃²⁻ concentrations. In these particular conditions, which occurred towards the end of
632 the tidal emersion period, any CaCO₃ precipitation was less than dissolution; precipitation may
633 even have been impossible due to a lack of DIC substrate. In intertidal pools with a high density
634 of *Zostera marina*, Miller & Kelley (2021) observed a similar decoupling between pH and Ω_a with
635 increases in pH not leading to an increase in saturation state at high pH values due to a lack of
636 DIC/CO₃²⁻. In our study, we observed even more drastic decoupling between expected changes in
637 pH, Ω_a and NCC, with some of the fastest net dissolution rates observed at very high pH and very
638 low Ω_a values that were a consequence of near complete consumption of DIC by community



639 production (**Fig. 7**). Macroalgae cultivation has been proposed as a method of bioremediation to
640 local acidification, in particular to improve aquaculture environments (e.g., Bergstrom et al., 2019;
641 Gao & Beardall, 2022): increase in algal or marine plant cover would reverse or buffer the negative
642 effects of acidification on heterotroph calcifiers. Our results and those of Miller & Kelley (2021)
643 suggest that phytoremediation should not consider pH as the sole indicator for “acidification
644 remediation”, and that periodical decreases in saturation state in macroalgae- or seaweed-
645 dominated environments in summer (and during marine heatwaves), may need to be considered
646 for these proposed types of remediations.

647

648 **Conclusion**

649 Relative to its area, human societies are disproportionately reliant on the coastal ocean for the
650 provision of natural resources and climate regulation. Yet our understanding of how anthropogenic
651 carbon emissions and associated ocean acidification will influence natural coastal ecosystems and
652 community metabolism remains limited. In the present study, we manipulated the carbonate
653 chemistry of natural temperate intertidal pools to explore the potential impact of future ocean
654 acidification on community-level calcification and production. We find evidence of large seasonal,
655 diel and community-specific differences in the sensitivity of intertidal community metabolism to
656 acidification. Diurnally, acidification was found to enhance net community production, with this
657 “fertilization effect” indicating algal photosynthesis is naturally carbon limited in such
658 environments at emersion. Diurnal net community calcification was unaffected by acidification.
659 In contrast, nocturnal acidification resulted in greater net community dissolution in the intertidal
660 pools yet had no consistent effect on community respiration. Integrated over day/night emersion
661 periods, the intertidal mesocosms maintained positive net community calcification and production
662 under both present-day and future conditions. Albeit considerable differences between individual
663 pools and strong seasonal dependencies, our results indicate that the net calcification and
664 production of temperate intertidal communities - likely acclimated/adapted to variable conditions
665 - could be affected by future acidification.

666

667 **ACKNOWLEDGEMENTS**



668 We thank Elsa Perruchini, Léonard Dupont, Corentin Clerc, Priscilla Le Mezo, Alban Planchat,
669 Maud Chevalier, Anne Cornillon, Annabel Antheaume, Maïlys Roux and Clarisse Dufaux for their
670 kind assistance with fieldwork. This project is fully funded by the CHANEL research chair:
671 *Understanding the Linkages between the Ocean, the Carbon Cycle, and Marine Ecosystems under*
672 *Climate Change*. Data presented for adjacent Atlantic waters characteristics (main text and the
673 supplementary material) were kindly provided by the SOMLIT network database (Service
674 d’Observation en Milieu Littoral; www.somlit.fr) on June 2022.

675

676 **AUTHORS CONTRIBUTIONS**

677 ND, SM and LK designed the experiments and ND carried them out with help from all co-authors.
678 ND analysed the data and prepared the manuscript, with contributions from all co-authors.

679

680 **COMPETING INTERESTS**

681 The authors declare that they have no conflict of interest.

682

683 **DATA AVAILABILITY**

684 Raw data and linear regression model results are provided as supplementary in the Appendix.

685



686 **BIBLIOGRAPHY:**

- 687 Albright, R., Caldeira, L., Hosfelt, J., Kwiatkowski, L., Maclaren, J. K., Mason, B. M., Nebuchina, Y.,
688 Ninokawa, A., Pongratz, J., Ricke, K. L., Rivlin, T., Schneider, K., Sesboüé, M., Shamberger, K.,
689 Silverman, J., Wolfe, K., Zhu, K., & Caldeira, K. (2016). Reversal of ocean acidification
690 enhances net coral reef calcification. *Nature*, 531(7594), Article 7594.
691 <https://doi.org/10.1038/nature17155>
- 692 Albright, R., Takeshita, Y., Koweek, D. A., Ninokawa, A., Wolfe, K., Rivlin, T., Nebuchina, Y., Young,
693 J., & Caldeira, K. (2018). Carbon dioxide addition to coral reef waters suppresses net community
694 calcification. *Nature*, 555(7697), Article 7697. <https://doi.org/10.1038/nature25968>
- 695 Aminot, A., & K erouel, R. (2007). *Dosage automatique des nutriments dans les eaux marines: M ethodes*
696 *en flux continu*. Editions Quae.
- 697 Andersson, A. J., Kline, D. I., Edmunds, P. J., Archer, S. D., Bednar sek, N., Carpenter, R. C., Chadsey,
698 M., Goldstein, P., Grotoli, A. G., Hurst, T. P., King, A. L., K ubler, J. E., Kuffner, I. B., Mackey,
699 K. R. M., Menge, B. A., Paytan, A., Riebesell, U., Schnetzer, A., Warner, M. E., & Zimmerman,
700 R. C. (2015). Understanding ocean acidification impacts on organismal to ecological scales.
701 *Oceanography*, 28(2), 16–27.
- 702 Barry, J., Hall-Spencer, J., & Tyrrell, T. (2010). In situ perturbation experiments: Natural venting sites,
703 spatial/temporal gradients in ocean pH, manipulative in situ $p\text{CO}_2$ perturbations. In *Guide to best*
704 *practices in ocean acidification research and data reporting* (pp. 123–136).
- 705 Bergstrom, E., Silva, J., Martins, C., & Horta, P. (2019). Seagrass can mitigate negative ocean
706 acidification effects on calcifying algae. *Scientific Reports*, 9(1), Article 1.
707 <https://doi.org/10.1038/s41598-018-35670-3>
- 708 Borowitzka, M. A. (1981). Photosynthesis and calcification in the articulated coralline red algae
709 *Amphiroa anceps* and *A. foliacea*. *Marine Biology*, 62(1), 17–23.
710 <https://doi.org/10.1007/BF00396947>



- 711 Bracken, M. E. S., Miller, L. P., Mastroni, S. E., Lira, S. M., & Sorte, C. J. B. (2022). Accounting for
712 variation in temperature and oxygen availability when quantifying marine ecosystem metabolism.
713 *Scientific Reports*, 12:825, Article 1. <https://doi.org/10.1038/s41598-021-04685-8>
- 714 Cocquempot, L., Delacourt, C., Paillet, J., Riou, P., Aucan, J., Castelle, B., Charria, G., Claudet, J.,
715 Conan, P., Coppola, L., Hocdé, R., Planes, S., Raimbault, P., Savoye, N., Testut, L., & Vuillemin,
716 R. (2019). Coastal ocean and nearshore observation: A French case study. *Frontiers in Marine*
717 *Science*, 6. <https://doi.org/10.3389/fmars.2019.00324>
- 718 Comeau, S., Carpenter, R. C., & Edmunds, P. J. (2013). Coral reef calcifiers buffer their response to
719 ocean acidification using both bicarbonate and carbonate. *Proceedings of the Royal Society B:*
720 *Biological Sciences*, 280(1753), 20122374. <https://doi.org/10.1098/rspb.2012.2374>
- 721 Cox, T. E., Schenone, S., Delille, J., Diaz-Castañeda, V., Alliouane, S., Gattuso, J.-P., & Gazeau, F.
722 (2015). Effects of ocean acidification on *Posidonia oceanica* epiphytic community and shoot
723 productivity. *Journal of Ecology*, 103(6), 1594–1609. <https://doi.org/10.1111/1365-2745.12477>
- 724 Dickson, A., Sabine, C. L., & Christian, J. R. (2007). *Guide to best practices for ocean CO₂*
725 *measurements*. PICES Special Publication 3; 191 pp.
- 726 Dorey, N., Lançon, P., Thorndyke, M., & Dupont, S. (2013). Assessing physiological tipping point of sea
727 urchin larvae exposed to a broad range of pH. *Global Change Biology*, 19(11), 3355–3367.
728 <https://doi.org/10.1111/gcb.12276>
- 729 Egilsdottir, H., Noisette, F., Noël, L. M.-L. J., Olafsson, J., & Martin, S. (2013). Effects of *p*CO₂ on
730 physiology and skeletal mineralogy in a tidal pool coralline alga *Corallina elongata*. *Marine*
731 *Biology*, 160(8), 2103–2112. <https://doi.org/10.1007/s00227-012-2090-7>
- 732 Foo, S., Byrne, M., Ricevuto, E., & Gambi, M. C. (2018). The carbon dioxide vents of Ischia, Italy, a
733 natural system to assess impacts of ocean acidification on marine ecosystems: An overview of
734 research and comparisons with other vent systems. *Oceanography and Marine Biology: An*
735 *Annual Review*, 56, 237–310. <https://doi.org/10.1201/9780429454455-4>



- 736 Ganning, B. (1971). Studies on chemical, physical and biological conditions in swedish rockpool
737 ecosystems. *Ophelia*, 9(1), 51–105. <https://doi.org/10.1080/00785326.1971.10430090>
- 738 Gao, K., & Beardall, J. (2022). Using macroalgae to address UN Sustainable Development goals through
739 CO₂ remediation and improvement of the aquaculture environment. *Applied Phycology*, 3(1),
740 360–367. <https://doi.org/10.1080/26388081.2022.2025617>
- 741 Gattuso, J.-P., Epitalon, J.-M., Lavigne, H., & Orr, J. (2021). *seacarb: Seawater carbonate chemistry with*
742 *R. R package version 3.2.16* <http://CRAN.R-project.org/package=seacarb>.
- 743 Gazeau, F., Urbini, L., Cox, T., Alliouane, S., & Gattuso, J. (2015). Comparison of the alkalinity and
744 calcium anomaly techniques to estimate rates of net calcification. *Marine Ecology Progress*
745 *Series*, 527, 1–12. <https://doi.org/10.3354/meps11287>
- 746 Gran, G. (1952). Determination of the equivalence point in potentiometric titrations. Part II. *The Analyst*,
747 77(920), 661. <https://doi.org/10.1039/an9527700661>
- 748 Haraldsson, C., Anderson, L. G., Hassellöv, M., Hulth, S., & Olsson, K. (1997). Rapid, high-precision
749 potentiometric titration of alkalinity in ocean and sediment pore waters. *Deep Sea Research Part*
750 *I: Oceanographic Research Papers*, 44(12), 2031–2044. [https://doi.org/10.1016/S0967-](https://doi.org/10.1016/S0967-0637(97)00088-5)
751 0637(97)00088-5
- 752 Houlihan, E. P., Espinel-Velasco, N., Cornwall, C. E., Pilditch, C. A., & Lamare, M. D. (2020). Diffusive
753 boundary layers and ocean acidification: Implications for sea urchin settlement and growth.
754 *Frontiers in Marine Science*, 7. <https://www.frontiersin.org/articles/10.3389/fmars.2020.577562>
- 755 Hurd, C. L., Beardall, J., Comeau, S., Cornwall, C. E., Havenhand, J. N., Munday, P. L., Parker, L. M.,
756 Raven, J. A., McGraw, C. M., Hurd, C. L., Beardall, J., Comeau, S., Cornwall, C. E., Havenhand,
757 J. N., Munday, P. L., Parker, L. M., Raven, J. A., & McGraw, C. M. (2019). Ocean acidification
758 as a multiple driver: How interactions between changing seawater carbonate parameters affect
759 marine life. *Marine and Freshwater Research*, 71(3), 263–274. <https://doi.org/10.1071/MF19267>



- 760 IPCC. (2019). *IPCC Special Report on the Ocean and Cryosphere in a Changing Climate* (H. O. Pörtner,
761 D. Roberts, V. Masson-Delmotte, & P. Zhai, Eds.). Cambridge University Press, UK.
762 <https://doi.org/10.1017/9781009157964>
- 763 Jia, G., E. Shevliakova, P. Artaxo, N. De Noblet-Ducoudré, R. Houghton, J. House, K. Kitajima, C.
764 Lennard, A. Popp, A. Sirin, R. Sukumar, & L. Verchot. (2019). Land–climate interactions. In
765 *Climate Change and Land: An IPCC special report on climate change, desertification, land*
766 *degradation, sustainable land management, food security, and greenhouse gas fluxes in*
767 *terrestrial ecosystems* (P.R. Shukla, J. Skea, E. Calvo Buendia, V. Masson-Delmotte, H.-O.
768 Pörtner, D.C. Roberts, P. Zhai, R. Slade, S. Connors, R. van Diemen, M. Ferrat, E. Haughey, S.
769 Luz, S. Neogi, M. Pathak, J. Petzold, J. Portugal Pereira, P. Vyas, E. Huntley, K. Kissick, M.
770 Belkacemi, J. Malley). <https://www.ipcc.ch/srccl/chapter/chapter-2/>
- 771 Johnson, M. D., Moriarty, V. W., & Carpenter, R. C. (2014). Acclimatization of the Crustose Coralline
772 Alga *Porolithon* onkodes to Variable pCO₂. *PLOS ONE*, 9(2), e87678.
773 <https://doi.org/10.1371/journal.pone.0087678>
- 774 Kottmeier, D. M., Chrachri, A., Langer, G., Helliwell, K. E., Wheeler, G. L., & Brownlee, C. (2022).
775 Reduced H⁺ channel activity disrupts pH homeostasis and calcification in coccolithophores at
776 low ocean pH. *Proceedings of the National Academy of Sciences*, 119(19), e2118009119.
777 <https://doi.org/10.1073/pnas.2118009119>
- 778 Kroeker, K. J., Micheli, F., & Gambi, M. C. (2012). Ocean acidification causes ecosystem shifts via
779 altered competitive interactions. *Nature Climate Change*, 3(2), 156–159.
780 <https://doi.org/10.1038/nclimate1680>
- 781 Kwiatkowski, L., Gaylord, B., Hill, T., Hosfelt, J., Kroeker, K. J., Nebuchina, Y., Ninokawa, A., Russell,
782 A. D., Rivest, E. B., Sesboué, M., & Caldeira, K. (2016). Nighttime dissolution in a temperate
783 coastal ocean ecosystem increases under acidification. *Scientific Reports*, 6(1), Article 1.
784 <https://doi.org/10.1038/srep22984>



- 785 Kwiatkowski, L., Torres, O., Bopp, L., Aumont, O., Chamberlain, M., Christian, J. R., Dunne, J. P.,
786 Gehlen, M., Ilyina, T., John, J. G., Lenton, A., Li, H., Lovenduski, N. S., Orr, J. C., Palmieri, J.,
787 Santana-Falcón, Y., Schwinger, J., Séférian, R., Stock, C. A., ... Ziehn, T. (2020). Twenty-first
788 century ocean warming, acidification, deoxygenation, and upper-ocean nutrient and primary
789 production decline from CMIP6 model projections. *Biogeosciences*, 17(13), 3439–3470.
790 <https://doi.org/10.5194/bg-17-3439-2020>
- 791 Legrand, E., Riera, P., Lutier, M., Coudret, J., Grall, J., & Martin, S. (2019). Grazers increase the
792 sensitivity of coralline algae to ocean acidification and warming. *Journal of Sea Research*, 148–
793 149, 1–7. <https://doi.org/10.1016/j.seares.2019.03.001>
- 794 Legrand, E., Riera, P., Pouliquen, L., Bohner, O., Cariou, T., & Martin, S. (2018). Ecological
795 characterization of intertidal rockpools: Seasonal and diurnal monitoring of physico-chemical
796 parameters. *Regional Studies in Marine Science*, 17, 1–10.
797 <https://doi.org/10.1016/j.rsma.2017.11.003>
- 798 Mackey, K. R. M., Morris, J. J., Morel, F. M. M., & Kranz, S. A. (2015). Response of photosynthesis to
799 ocean acidification. *Oceanography*, 28(2), 74–91.
- 800 Martin, S., Charnoz, A., & Gattuso, J.-P. (2013). Photosynthesis, respiration and calcification in the
801 Mediterranean crustose coralline alga *Lithophyllum cabiochae* (Corallinales, Rhodophyta).
802 *European Journal of Phycology*, 48(2), 163–172. <https://doi.org/10.1080/09670262.2013.786790>
- 803 Martin, S., Cohu, S., Vignot, C., Zimmerman, G., & Gattuso, J.-P. (2013). One-year experiment on the
804 physiological response of the Mediterranean crustose coralline alga, *Lithophyllum cabiochae*, to
805 elevated $p\text{CO}_2$ and temperature. *Ecology and Evolution*, 3(3), 676–693.
806 <https://doi.org/10.1002/ece3.475>
- 807 Miller, C. A., & Kelley, A. L. (2021). Alkalinity cycling and carbonate chemistry decoupling in seagrass
808 mystify processes of acidification mitigation. *Scientific Reports*, 11:13500.
809 <https://doi.org/10.1038/s41598-021-92771-2>



- 810 Morris, S., & Taylor, A. C. (1983). Diurnal and seasonal variation in physico-chemical conditions within
811 intertidal rock pools. *Estuarine, Coastal and Shelf Science*, 17(3), 339–355.
812 [https://doi.org/10.1016/0272-7714\(83\)90026-4](https://doi.org/10.1016/0272-7714(83)90026-4)
- 813 Noisette, F., Egilsdottir, H., Davoult, D., & Martin, S. (2013). Physiological responses of three temperate
814 coralline algae from contrasting habitats to near-future ocean acidification. *Journal of*
815 *Experimental Marine Biology and Ecology*, 448, 179–187.
816 <https://doi.org/10.1016/j.jembe.2013.07.006>
- 817 Paiva, F., Brennecke, D., Pansch, C., & Briski, E. (2021). Consistency of aquatic enclosed experiments:
818 The importance of scale and ecological complexity. *Diversity and Distributions*, 27(3), 524–532.
- 819 Pan, T.-C. F., Applebaum, S. L., & Manahan, D. T. (2015). Experimental ocean acidification alters the
820 allocation of metabolic energy. *Proceedings of the National Academy of Sciences of the United*
821 *States of America*, 112(15), 4696–4701. <https://doi.org/10.1073/pnas.1416967112>
- 822 Pansch, A., Winde, V., Asmus, R., & Asmus, H. (2016). Tidal benthic mesocosms simulating future
823 climate change scenarios in the field of marine ecology. *Limnology and Oceanography: Methods*,
824 14(4), 257–267. <https://doi.org/10.1002/lom3.10086>
- 825 Pinheiro, J., Bates, D., & R-core. (2018). Package “nlme”: Linear and Nonlinear Mixed Effects Models.
826 In *Cran-R*.
- 827 R Core Team. (2017). R: A language and environment for statistical computing. In *R: A language and*
828 *environment for statistical computing*. <https://www.r-project.org/>
- 829 Raven, J. A. (2011). Effects on marine algae of changed seawater chemistry with increasing atmospheric
830 CO₂. *Biology and Environment: Proceedings of the Royal Irish Academy*, 111B(1), 1–17.
- 831 Riebesell, U., Czerny, J., von Bröckel, K., Boxhammer, T., Büdenbender, J., Deckelnick, M., Fischer, M.,
832 Hoffmann, D., Krug, S. A., Lentz, U., Ludwig, A., Mucche, R., & Schulz, K. G. (2013). Technical
833 Note: A mobile sea-going mesocosm system – new opportunities for ocean change research.
834 *Biogeosciences*, 10(3), 1835–1847. <https://doi.org/10.5194/bg-10-1835-2013>



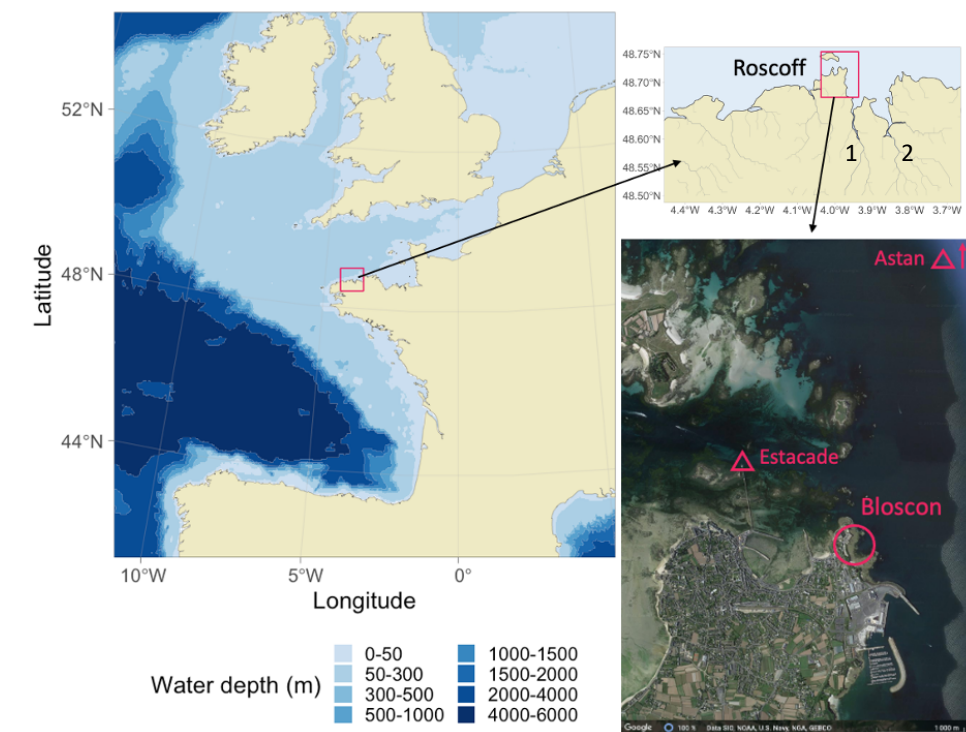
- 835 Ries, J. B. (2011). Skeletal mineralogy in a high-CO₂ world. *Journal of Experimental Marine Biology and*
836 *Ecology*, 403(1–2), 54–64. <https://doi.org/10.1016/j.jembe.2011.04.006>
- 837 Ries, J. B., Ghazaleh, M. N., Connolly, B., Westfield, I., & Castillo, K. D. (2016). Impacts of seawater
838 saturation state ($\Omega_A=0.4\text{--}4.6$) and temperature (10, 25°C) on the dissolution kinetics of whole-
839 shell biogenic carbonates. *Geochimica et Cosmochimica Acta*, 192, 318–337.
840 <https://doi.org/10.1016/j.gca.2016.07.001>
- 841 Schulz, K. G., Bellerby, R. G. J., Brussaard, C. P. D., Büdenbender, J., Czerny, J., Engel, A., Fischer, M.,
842 Koch-Klavsen, S., Krug, S. A., Lischka, S., Ludwig, A., Meyerhöfer, M., Nondal, G., Silyakova,
843 A., Stuhr, A., & Riebesell, U. (2013). Temporal biomass dynamics of an Arctic plankton bloom
844 in response to increasing levels of atmospheric carbon dioxide. *Biogeosciences*, 10(1), 161–180.
845 <https://doi.org/10.5194/bg-10-161-2013>
- 846 Smith, S. V., & Key, G. S. (1975). Carbon dioxide and metabolism in marine environments. *Limnology*
847 *and Oceanography*, 20(3), 493–495. <https://doi.org/10.4319/lo.1975.20.3.0493>
- 848 Spisla, C., Taucher, J., Bach, L. T., Haunost, M., Boxhammer, T., King, A. L., Jenkins, B. D., Wallace, J.
849 R., Ludwig, A., Meyer, J., Stange, P., Minutolo, F., Lohbeck, K. T., Nauendorf, A., Kalter, V.,
850 Lischka, S., Sswat, M., Dörner, I., Ismar-Rebitz, S. M. H., ... Riebesell, U. (2021). Extreme
851 levels of ocean acidification restructure the plankton community and biogeochemistry of a
852 temperate coastal ecosystem: A mesocosm study. *Frontiers in Marine Science*, 7:611157.
853 <https://www.frontiersin.org/articles/10.3389/fmars.2020.611157>
- 854 Stumpp, M., Hu, M. Y., Casties, I., Saborowski, R., Bleich, M., Melzner, F., & Dupont, S. (2013).
855 Digestion in sea urchin larvae impaired under ocean acidification. *Nature Climate Change*, 3(12),
856 1044–1049. <https://doi.org/10.1038/nclimate2028>
- 857 Sulpis, O., Jeansson, E., Dinauer, A., Lauvset, S. K., & Middelburg, J. J. (2021). Calcium carbonate
858 dissolution patterns in the ocean. *Nature Geoscience*, 14(6), Article 6.
859 <https://doi.org/10.1038/s41561-021-00743-y>



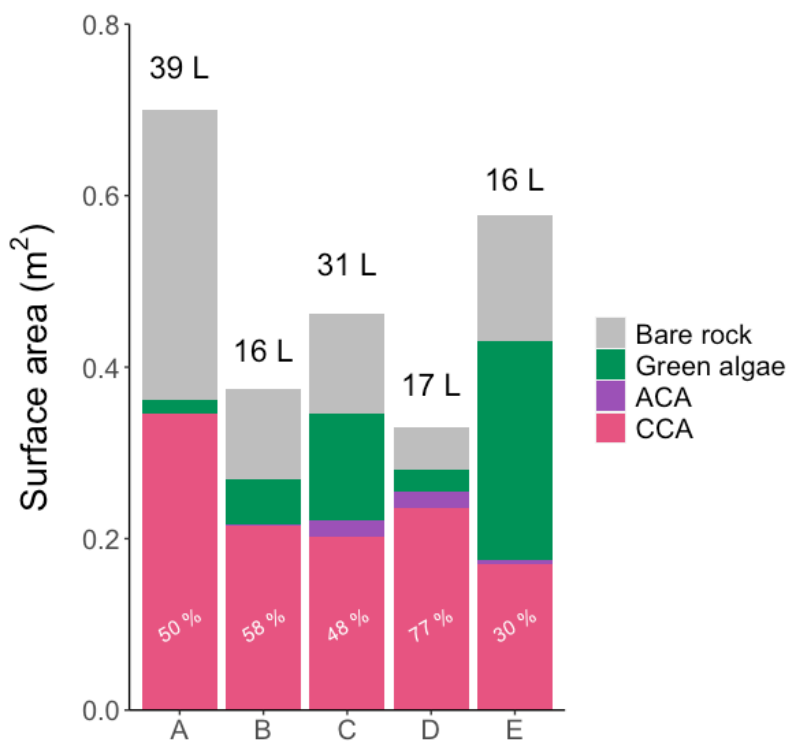
- 860 Sulpis, O., Lauvset, S. K., & Hagens, M. (2020). Current estimates of K_1^* and K_2^* appear inconsistent
861 with measured CO_2 system parameters in cold oceanic regions. *Ocean Science*, 16(4), 847–862.
862 <https://doi.org/10.5194/os-16-847-2020>
- 863 Torres, O., Kwiatkowski, L., Sutton, A. J., Dorey, N., & Orr, J. C. (2021). Characterizing mean and
864 extreme diurnal variability of ocean CO_2 system variables across marine environments.
865 *Geophysical Research Letters*, 48(5), e2020GL090228. <https://doi.org/10.1029/2020GL090228>
- 866 Widdicombe, S., Dupont, S., & Thorndyke, M. (2010). Laboratory experiments and benthic mesocosm
867 studies. In *Guide to best practices for ocean acidification research and data reporting*. U.
868 Riebesell, V. J. Fabry, L. Hansson and J.-P. Gattuso. Publications Office of the European Union.
- 869 Williamson, C. J., Perkins, R., Voller, M., Yallop, M. L., & Brodie, J. (2017). The regulation of coralline
870 algal physiology, an in situ study of *Corallina officinalis* (Corallinales, Rhodophyta).
871 *Biogeosciences*, 14(19), 4485–4498. <https://doi.org/10.5194/bg-14-4485-2017>
- 872 Yamamoto, S., Kayanne, H., Terai, M., Watanabe, A., Kato, K., Negishi, A., & Nozaki, K. (2012).
873 Threshold of carbonate saturation state determined by CO_2 control experiment. *Biogeosciences*,
874 9(4), 1441–1450. <https://doi.org/10.5194/bg-9-1441-2012>
- 875



1 Figures with legends -



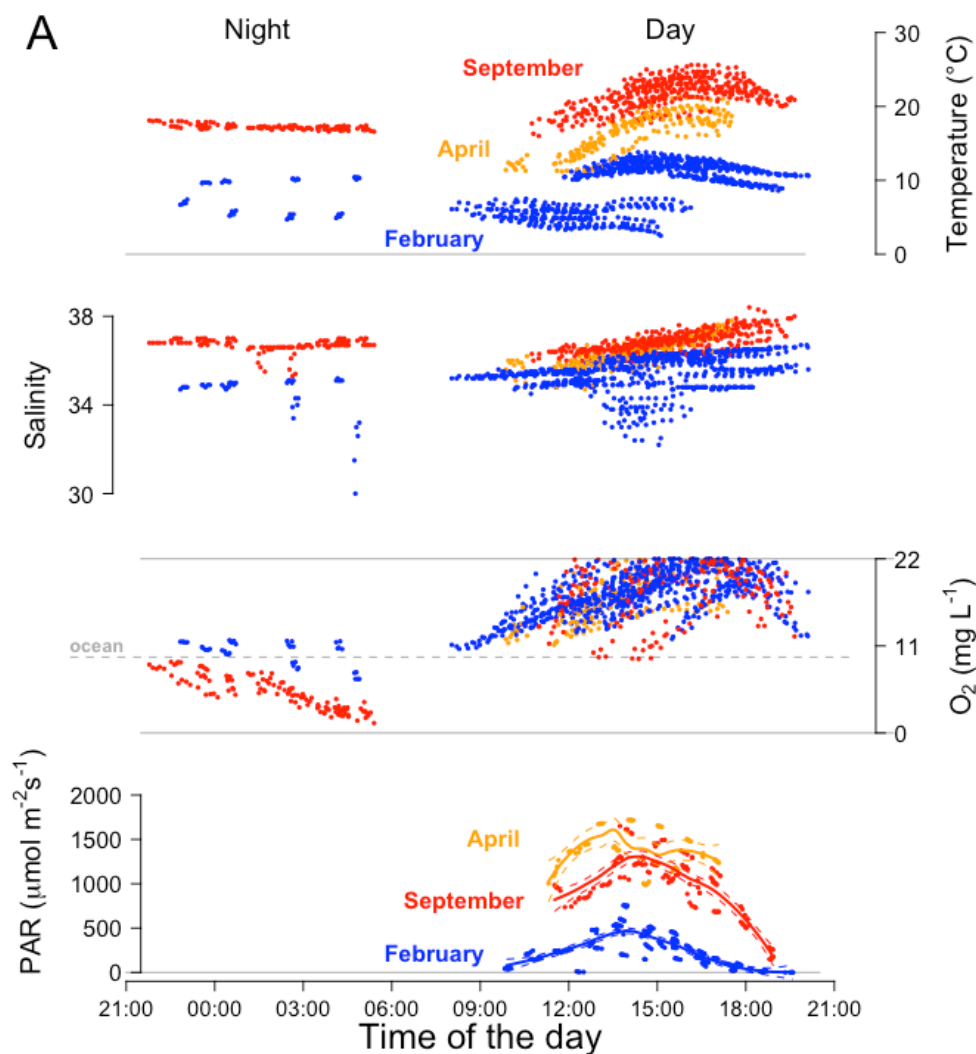
- 2 **Figure 1 - Field site location** on a map of Europe (left). The study site (Bloscon) is located in Roscoff,
- 3 Brittany, France (right, top: river mapping data from *HydroSHEDS*, 1. Penzé river and 2. Morlaix
- 4 river; bottom: satellite image from © *Google Earth*: earth.google.com/web/, acquired in June 2022).
- 5 The SOMLIT stations Astan and Estacade are indicated with triangles (www.somlit.fr).

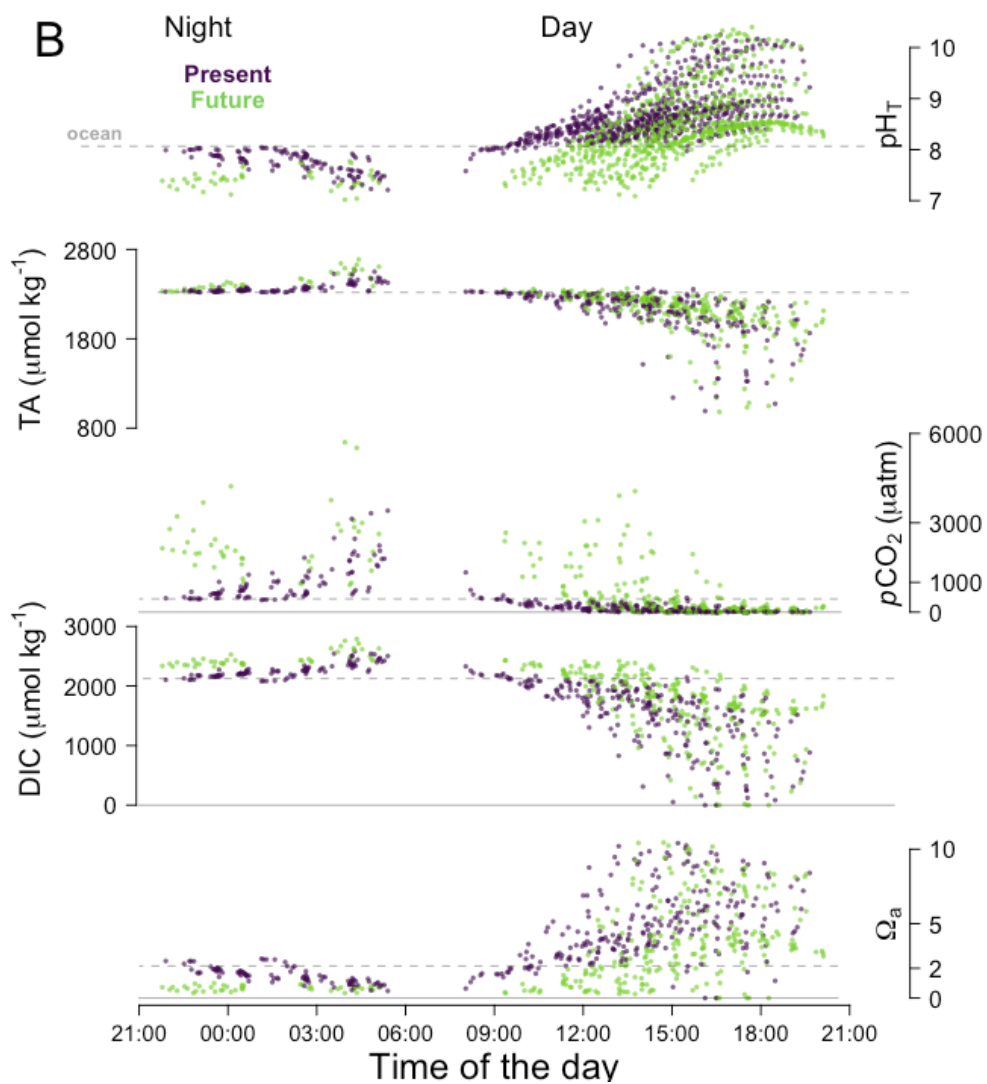


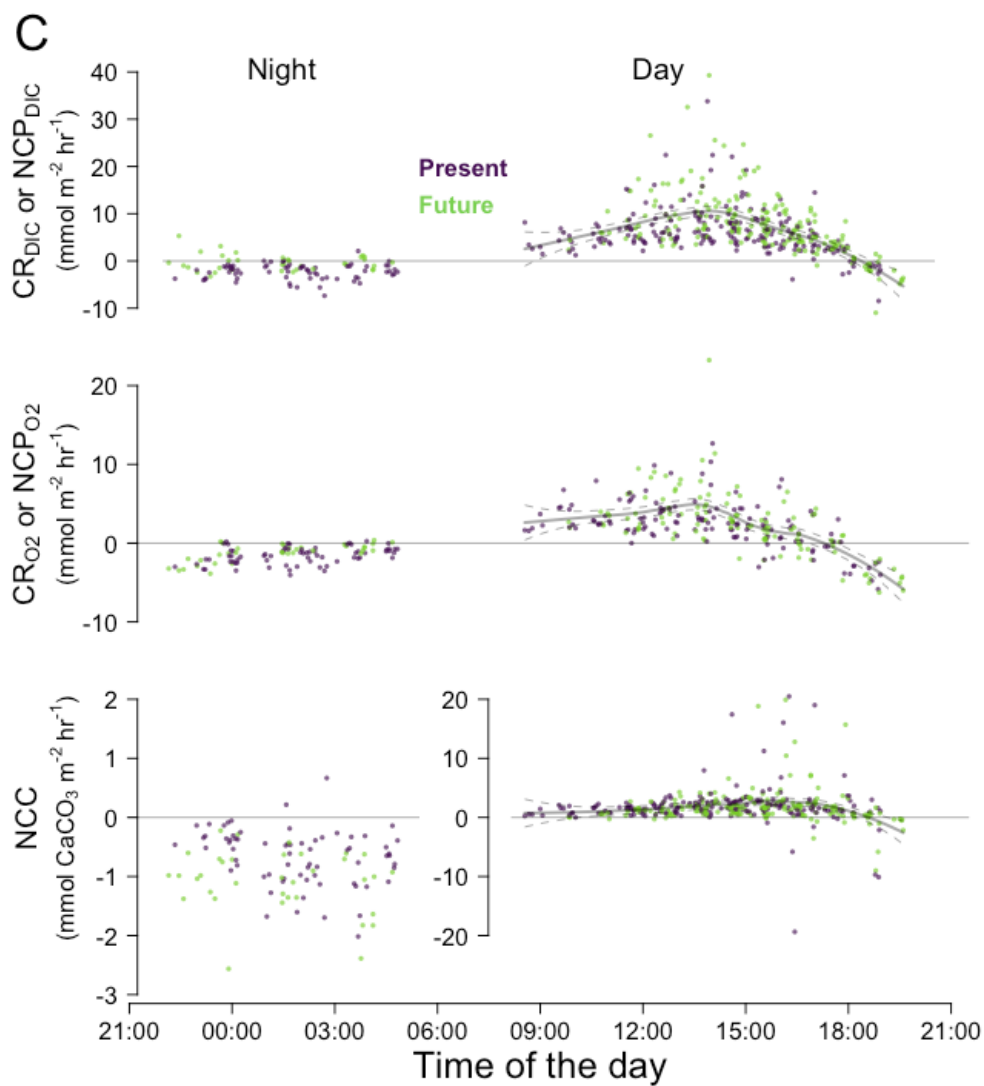
7 **Figure 2 - Pool area, volume and coverage** - Surface of the five pools (A-E, September 2020) covered
8 by crustose coralline algae (CCA, pink), articulated coralline algae (ACA, purple) and green algae
9 (green) or free of algae (“bare rock”, grey). The length of the bars represents total pool surface area
10 (m²) and the volume of each pool (L) is indicated above. The relative coverage (%) of calcifying algae
11 (ACA + CCA) in each pool is given. Details for the other seasons are available in **Supp. Mat. Pools**
12 **Fig. SP1 and SP2.**



13 **Figure 3 - Composite daily pool conditions and biological activity for all pools. A) temperature**
14 **(°C), salinity and oxygen concentration (mg L⁻¹) and Photosynthetically Active Radiation (PAR,**
15 **μmol m⁻² s⁻¹), B) pH_T, Total Alkalinity (TA, μmol kg⁻¹), pCO₂ (μatm), dissolved inorganic carbon**
16 **(DIC, μmol kg⁻¹) and aragonite saturation state (Ω_a), and C) DIC and O₂-derived NCP or CR**
17 **(mmol C or O m⁻² hr⁻¹) and NCC (mmol CaCO₃ m⁻² hr⁻¹). Colors represent seasons (A: blue for**
18 **February, orange for April, red for September) and treatment (B and C: purple for “present” and green**
19 **for “future”). Horizontal dotted grey lines represent the mean values of the adjacent ocean. Curves**
20 **were fitted by season for PAR and for diurnal NCP and NCC using a local polynomial regression**
21 **(*loess*) with 95% confidence interval. Number of observations: n = 1551 for temperature, salinity and**
22 **pH_T, n = 1169 for oxygen concentration (data recorded < 22 mg L⁻¹) and n = 632 (hourly data) for the**
23 **carbonate chemistry parameters, NCC and NCP or CR (B). All pools are shown.**





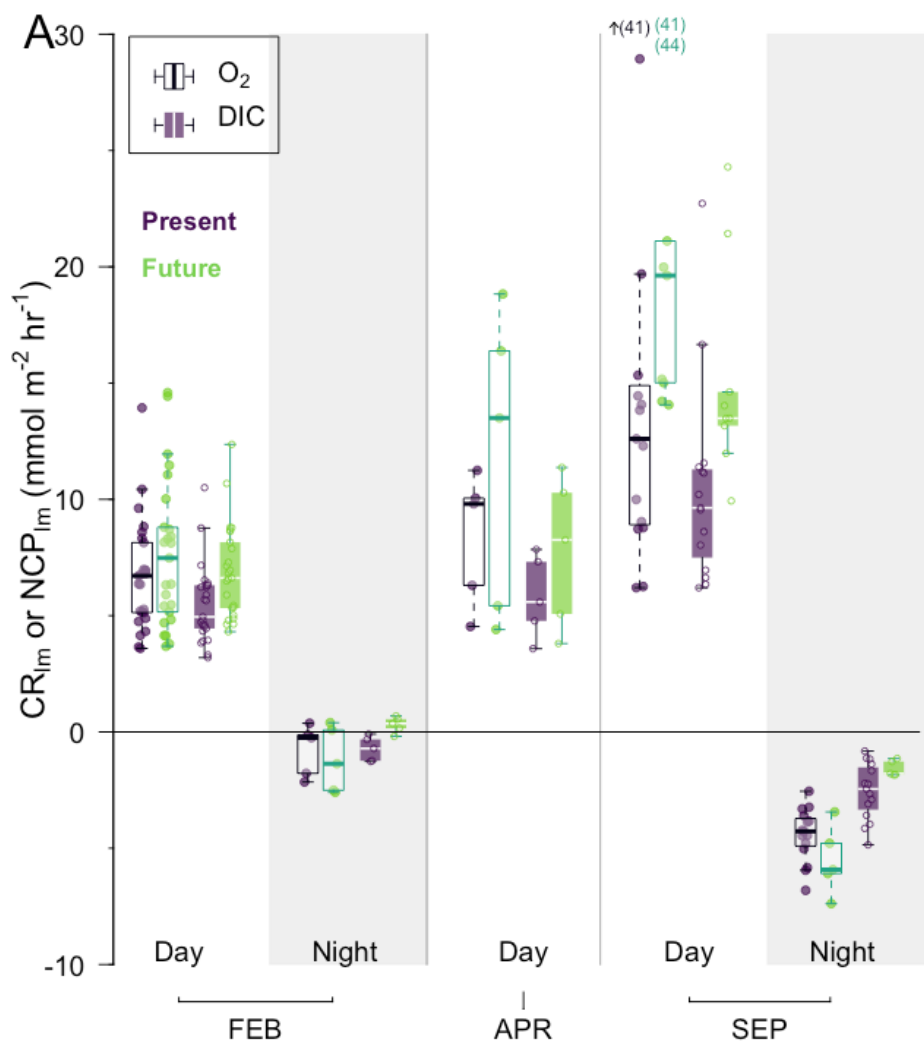


26

27

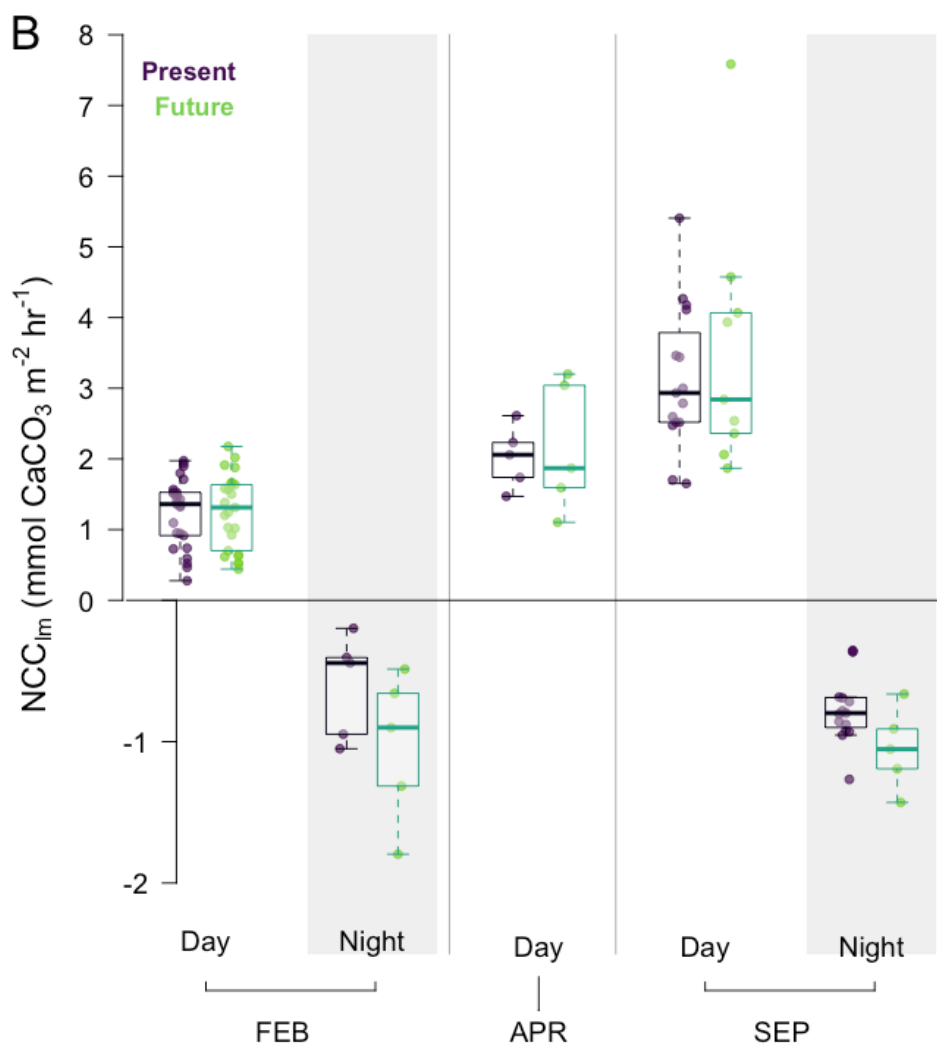


28 **Figure 4 – A) O_2 -derived (white boxes) and DIC-derived (colored boxes) NCP_{lm} ($mmol\ m^{-2}\ hr^{-1}$),**
 29 **and B) NCC_{lm} ($mmol\ CaCO_3\ m^{-2}\ hr^{-1}$) during the day and night (shaded areas), by season and**
 30 **by treatment** (purple for “present” and green for “future”) – Rates are presented as boxplots showing
 31 median, 1st and 3rd quartile and 1.5 inter-quartile range (bars), with overlaid individual observations
 32 (round symbols). Individual rates were calculated for each pool, each tide and each treatment: n = 50
 33 (FEB-day), n = 10 (FEB-night), n = 10 (APR-Day), n = 25 (SEP-Day), n = 20 (SEP-Night). Seasons:
 34 FEB for winter (pooled February 2020 and 2021), APR for spring (April 2021) and SEP for summer
 35 (pooled September 2020 and 2021). *Note that for NCC_{lm} , nights (<0) and days (>0) have different y-*
 36 *axis scales for better visualization of night differences. Statistical details of the linear regressions can*
 37 *be found in the corresponding **Supplementary Materials**. For O_2 -derived NCP_{lm} , in September, three*
 38 *rates were out of the range plotted and their values are indicated next to the small arrow.*



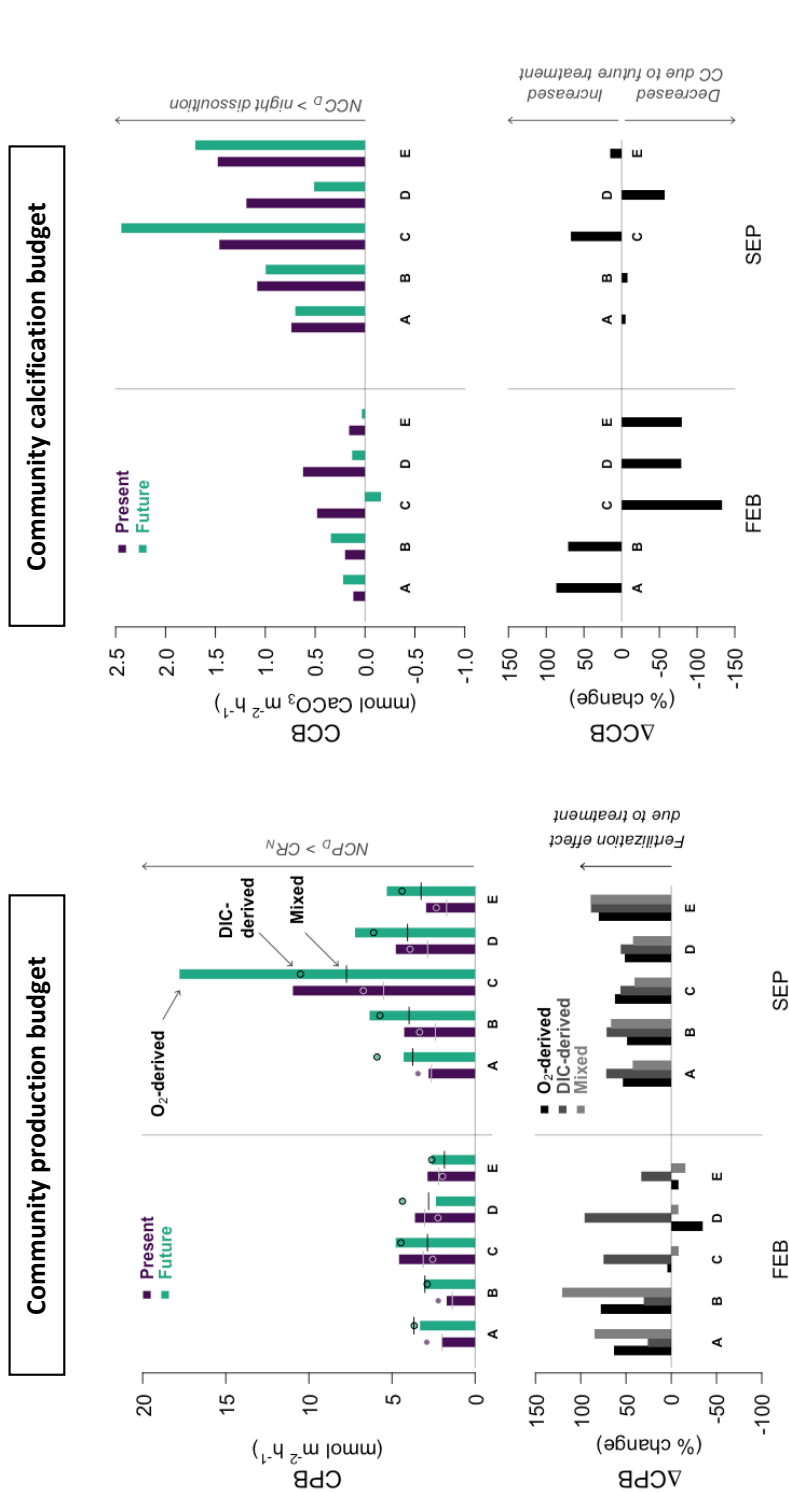
39

40

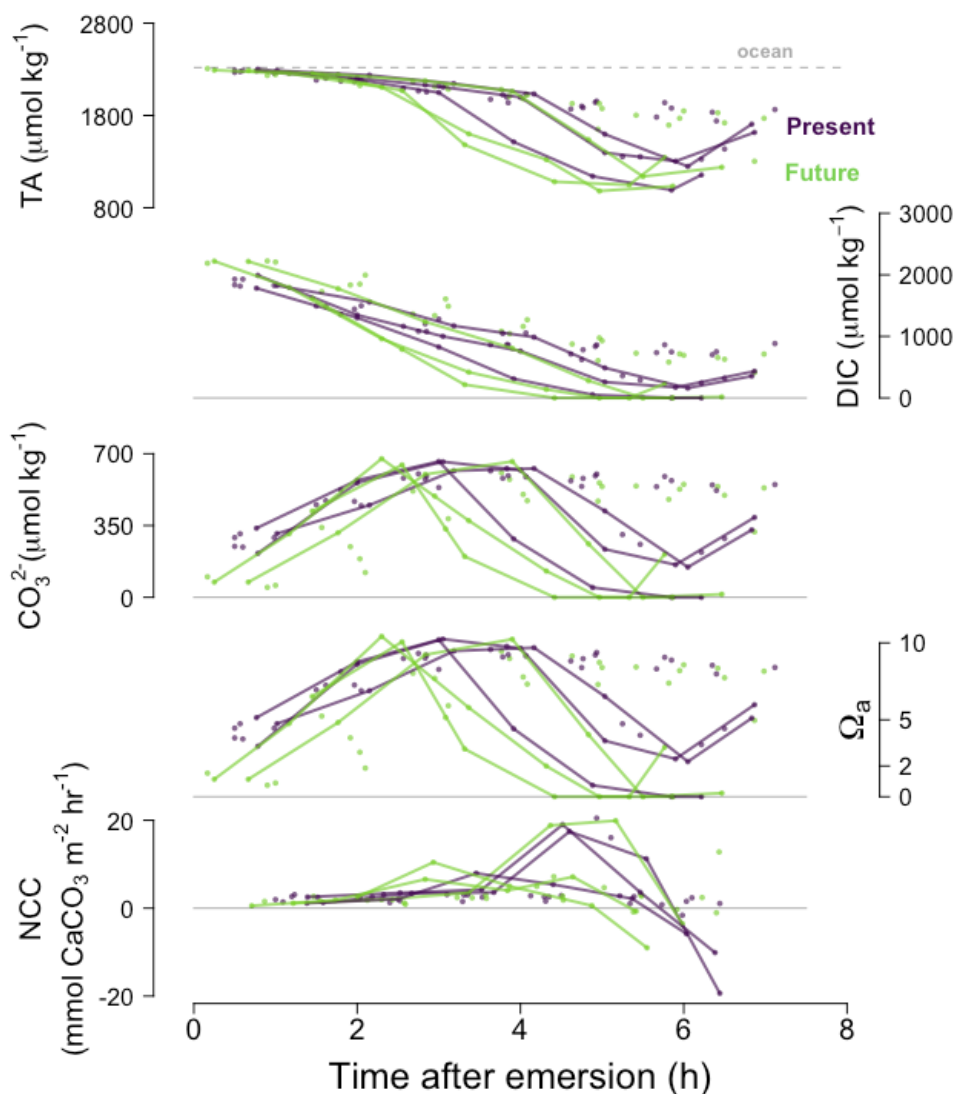


41

42



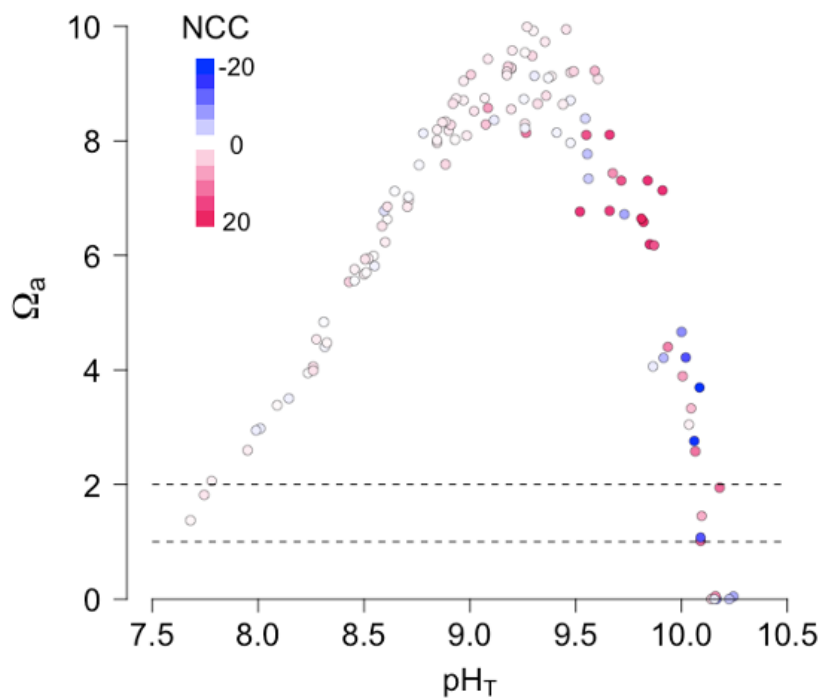
43 **Figure 5 – Community production budget: CPB_I), and calcification budget: CCB (upper right panel, $\text{mmol CaCO}_3 \text{ m}^{-2} \text{ hr}^{-1}$) by treatment**
 44 (purple for “present” and green for “future”) for each pool and season (same legend as Fig. 4). CPB > 0 if diurnal NCP > nocturnal respiration and
 45 CCB > 0 if diurnal NCC > nocturnal dissolution. CPB was estimated three different ways: from O₂-derived NCP (bars), from DIC-derived NCP
 46 (round symbols) and from nocturnal O₂-derived CR combined with diurnal DIC-derived NCP (“mixed”, vertical segments). **The bottom panels**
 47 **present the change (%) of diel production (ΔCPB: left) and diel calcification (ΔCCB: right) due to CO₂ addition.** Positive ΔCPB indicates
 48 a fertilization effect due to the CO₂ addition; negative ΔCCB is expected if the CO₂ addition decreases net calcification/increases net dissolution.
 49 All three methods to estimate CPB indicate a fertilization effect in summer.



50

51 **Figure 6 - Time series for September 2020 diurnal data only:** A) Total Alkalinity (TA, $\mu\text{mol kg}^{-1}$)
52 1), dissolved inorganic carbon, CO_3^{2-} concentration ($\mu\text{mol kg}^{-1}$), aragonite saturation state (Ω_a)
53 and NCC ($\text{mmol m}^{-2} \text{hr}^{-1}$) with time after emersion, by treatment (purple for “present” and green
54 for “future”). The lines in bold represent individual pools C and E that switched from calcification to
55 dissolution when pH_T was still above 9. A similar figure in **Supp. Mat. (Fig. S4)** shows that
56 sunset/irradiance are not correlated with the sudden change towards dissolution.

57



58 **Figure 7 – At very high pH there was both fast net calcification (red) and rapid net dissolution**
59 **(blue):** In some extreme cases, pH_T was not a good indicator of seawater saturation state (Ω_a). Selected
60 dataset of diurnal low-tide emersion periods from September 2020. Colors represent NCC (in mmol
61 $\text{CaCO}_3 \text{ m}^{-2} \text{ hr}^{-1}$, as presented in **Fig. 3C**). Dashed horizontal lines represent saturation state for
62 aragonite ($\Omega_a = 1$) and for high-Mg calcite ($\Omega_a = 2$).